AD-A116 253 ROCHESTER UNIV NY DEPT OF CHEMISTRY F/G 18/2
QUANTUM DYNAMICAL MODEL OF LASER-STIMULATED ISOTOPE SEPARATION --ETC(U)
JUN 82 J LIN, T F GEORGE N00014-80-C-0472
UNCLASSIFIED TR-20 NL

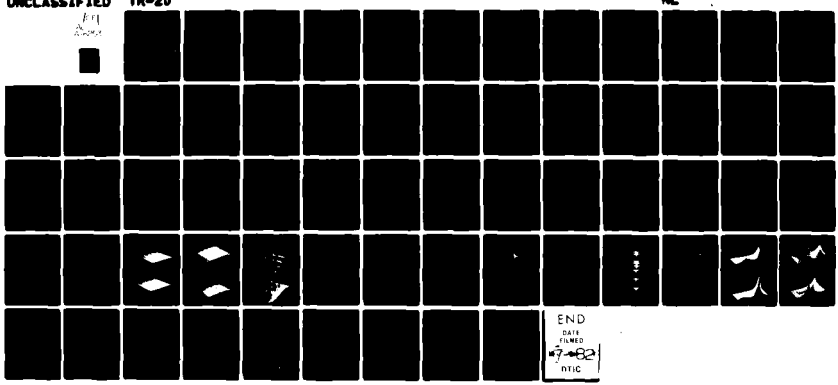

END
DATE FILMED
7-82
DTIC

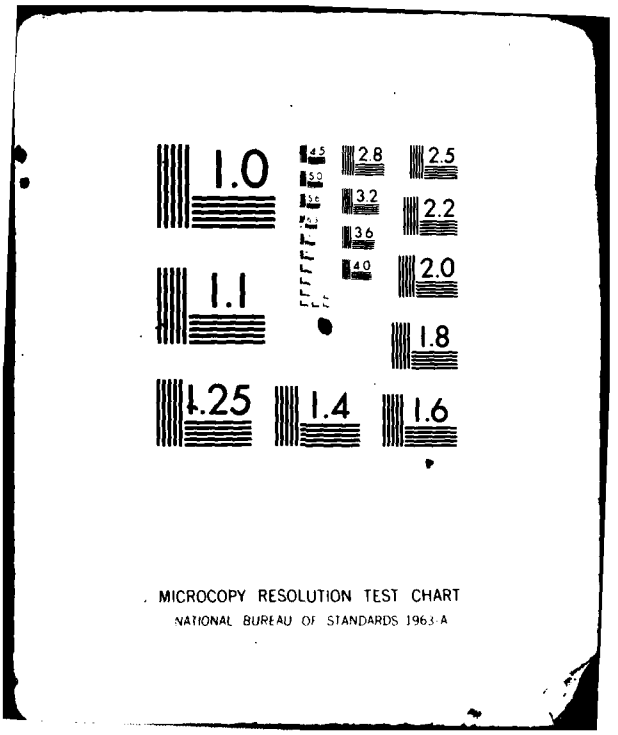
1.0
1.1
1.25
1.4
1.6
1.8
2.0
2.2
2.5
2.8
3.2
3.6
4.0
4.5
5.0
MICROCOPY RESOLUTION TEST CHART
NATIONAL BUREAU OF STANDARDS 1963-A

(12)

OFFICE OF NAVAL RESEARCH

Contract N00014-80-C-0472

Task No. NR 056-749

TECHNICAL REPORT No. 20

Quantum Dynamical Model of Laser-Stimulated Isotope Separation of Adsorbed Species: Role of Anharmonicity, Coupling Strength and Energy Feedback from the Heated Substrate

by

Jui-teng Lin and Thomas F. George

Prepared for Publication

in

Journal of Chemical Physics

University of Rochester
Department of Chemistry
Rochester, New York 14627

June, 1982

Unclassified

SECURITY CLASSIFICATION OF THIS PAGE (When Data Entered)

REPORT DOCUMENTATION PAGE	READ INSTRUCTIONS BEFORE COMPLETING FORM
1. REPORT NUMBER: 20	2. GOVT ACCESSION NO.: AD-A116 253
	3. RECIPIENT'S CATALOG NUMBER:
4. TITLE (and Subtitle): Quantum Dynamical Model of Laser-Stimulated Isotope Separation of Adsorbed Species: Role of Anharmonicity, Coupling Strength and Energy Feedback from the Heated Substrate	5. TYPE OF REPORT & PERIOD COVERED: Interim Technical Report
	6. PERFORMING ORG. REPORT NUMBER:
7. AUTHOR(s): Jui-teng Lin and Thomas F. George	8. CONTRACT OR GRANT NUMBER(s): N00014-80-C-0472
9. PERFORMING ORGANIZATION NAME AND ADDRESS: University of Rochester, Department of Chemistry, Rochester, New York 14627	10. PROGRAM ELEMENT, PROJECT, TASK AREA & WORK UNIT NUMBERS: NR 056-749
11. CONTROLLING OFFICE NAME AND ADDRESS: Office of Naval Research, Chemistry Program Code 472, Arlington, Virginia 22217	12. REPORT DATE: June, 1982
	13. NUMBER OF PAGES: 55
14. MONITORING AGENCY NAME & ADDRESS (if different from Controlling Office)	15. SECURITY CLASS. (of this report): Unclassified
	15a. DECLASSIFICATION/DOWNGRADING SCHEDULE

16. DISTRIBUTION STATEMENT (of this Report)

This document has been approved for public release and sale; its distribution is unlimited.

17. DISTRIBUTION STATEMENT (of the abstract entered in Block 20, if different from Report)

18. SUPPLEMENTARY NOTES

Prepared for publication in the Journal of Chemical Physics, in press.

19. KEY WORDS (Continue on reverse side if necessary and identify by block number)

ISOTOPE SEPARATION	PHONON-MEDIATED COUPLING
ADSORBED SPECIES	ENERGY FEEDBACK
QUANTUM MODEL	HEATED SUBSTRATE
ANHARMONICITY	PHASE RELAXATION
COUPLING STRENGTH	BISTABILITY

20. ABSTRACT (Continue on reverse side if necessary and identify by block number) A quantum model of a heterogeneous system consisting of a mixture of isotopes adsorbed on a solid surface and subjected to laser radiation is presented. The model system is described by a total Hamiltonian including direct and indirect (surface-phonon-mediated) couplings. The equations of motion are derived in the Heisenberg-Markoffian picture in which the many-body effects of the surface phonon modes and the ad-species are reduced to an overall broadening (damping factor) given by the sum of the energy (T_1) and phase (T_2) relaxations. The effects of the dephasing and anharmonicity on the average excitation are investigated. The "bistability"

DD FORM 1 JAN 73 1473 EDITION OF 1 NOV 65 IS OBSOLETE S/N 0102-LF-014-6601

Unclassified

SECURITY CLASSIFICATION OF THIS PAGE (When Data Entered)

feature with a red-shifted optimal detuning is discussed in terms of the solution of a cubic equation. A diagonalization procedure is presented in a new basis which reveals the effects of the coupling strength, the frequency difference and the level width of the isotopes on the total steady-state excitation, which in turn reflects the surface spectrum of the model system. Finally, the isotope selectivity given by the numerical results of the time-integrated excitations is discussed. It is shown that the optimal detuning for a weak coupling strength is further red-shifted for a strong isotopic coupling strength. Finally, energy feedback effects of the bath modes on the excitations of the active modes are investigated by combining a quantum excitation equation and a classical heat diffusion equation.

J. Chem. Phys., in press

Quantum Dynamical Model of Laser-Stimulated Isotope Separation of Adsorbed Species: Role of Anharmonicity, Coupling Strength and Energy Feedback from the Heated Substrate

Jui-teng Lin* and Thomas F. George
Department of Chemistry, University of Rochester
Rochester, New York 14627 U.S.A.

A quantum model of a heterogeneous system consisting of a mixture of isotopes adsorbed on a solid surface and subjected to laser radiation is presented. The model system is described by a total Hamiltonian including direct and indirect (surface-phonon-mediated) couplings. The equations of motion are derived in the Heisenberg-Markoffian picture in which the many-body effects of the surface phonon modes and the adspecies are reduced to an overall broadening (damping factor) given by the sum of the energy (T_1) and phase (T_2) relaxations. The effects of the dephasing and anharmonicity on the average excitation are investigated. The "bistability" feature with a red-shifted optimal detuning is discussed in terms of the solution of a cubic equation. A diagonalization procedure is presented in a new basis which reveals the effects of the coupling strength, the frequency difference and the level width of the isotopes on the total steady-state excitation, which in turn reflects the surface spectrum of the model system. Finally, the isotope selectivity given by the numerical results of the time-integrated excitations is discussed. It is shown that the optimal detuning for a weak coupling strength is further red-shifted for a strong isotopic coupling strength. Finally, energy feedback effects of the bath modes on the excitations of the active modes are investigated by combining a quantum excitation equation and a classical heat diffusion equation.

I. Introduction

Infrared multiphoton processes for the separation of isotopes in the gas phase have been widely studied both experimentally and theoretically in the past several years.[1] For a homogeneous gas-phase system, the selective separation of the isotopes is mainly characterized by the frequency difference of the isotopes resulting in different cross sections, and the coupling strength among the excited isotopes is governed by the gas pressure and concentrations of the species. For a heterogeneous system, e.g., isotopic species adsorbed on a solid surface, the energy transfer processes governing the selectivity of the isotope separation are more complicated due to the many-body effects of the adspecies and the surface/bulk atoms of the solid. Instead of pressure-induced collisions among the isotopes as in a homogeneous system, different interaction mechanisms are responsible for the energy transfer among the adspecies in a heterogeneous system. They include dipole-dipole interactions among the isotopes adsorbed at different lattice sites, migration-induced nonradiative interactions/collisions and other direct and indirect (surface-mediated) couplings.

For a system consisting of a group of identical adspecies and subjected to a laser radiation, the selective excitation of the active modes and/or the active species without significantly heating up the solid (phonon modes) has been recently studied by Lin et al.[2] In the present paper, we make the extension to a mixture of isotopes. The selectivity of the isotope separation is governed by the parameters involved in energy transfer processes such as the energy (T_1) and phase (T_2) relaxation rates, the coupling between the active

modes of the isotopes, the intra- and intermolecular couplings of the adspecies, the multiphonon relaxation rates of the active modes and their frequency difference resulting in different absorption cross sections.

The present paper is organized as follows. In Section II, a model system consisting of a group of mixed isotopes and subjected to laser radiation is described by a total vibrational Hamiltonian including the direct and indirect interactions among the active modes, which interact with each other and are coupled to a common bath comprised of the surface and bulk phonons (and also the inactive modes of the adspecies). The equations of motion of the average excitations (number of photons absorbed) are set up in the Heisenberg-Markoffian picture, and an excitation-dependent complex frequency resulting from the nonlinearity property of the excitation process is introduced in Section III. Two important features are shown in Section IV: (A) the effects of phase (T_2) relaxation on the time evolution of the average excitation, and (B) anharmonic effects on the steady-state excitation governed by a cubic equation, where the "bistability" characterized by a critical laser intensity and an optimal detuning are calculated exactly. The rise times of the steady-state excitation for laser frequencies far from as well as near the optimal detuning are graphically shown for the numerical solutions of the coupled equations. Anharmonic effects on the steady-state excitation and the bistability feature have been discussed in a previous paper,[3] but part of that discussion is repeated here for the sake of completeness. Furthermore, in the present paper we consider an alternative method, which includes

the dephasing effects on the transient excitation which were not calculated previously.[3]

In Section V, the role of the isotopic coupling strength played in the total excitation is analyzed, and expressions are derived for the level broadening (narrowing) and frequency red (blue) shift. The effects of the isotopic coupling strength, the frequency difference and the anharmonicity on the selectivity of isotope separation are investigated by means of numerical results of the time-integrated excitations in Section VI. Finally, we summarize the main results in Section VII.

II. Model Hamiltonian

We consider a model system consisting of an isotopic mixture of species adsorbed on a solid surface and subjected to infrared radiation with frequency near-resonant to those of the active modes of the system. The vibrational spectrum of the adspecies/surface system may be partitioned into a high-frequency region consisting of the active modes and the inactive modes of the adspecies and a low-frequency region comprised of the surface and bulk phonon modes. The latter are not optically active and can only be excited via multiphonon relaxation of the active modes. In addition to the irreversible energy transfer between the adspecies and the phonon modes, which presumably form a quasicontinuum, the reversible energy transfer among the intra- and interspecies bound states also plays a prime role in laser-stimulated surface processes. For a system consisting of a single polyatomic (n-atom) adspecies, the intra-species energy transfer is governed by the anharmonic coupling among

the 3n "frustrated" normal modes, and therefore the detailed energy populations in each individual mode involve solving a set of 3n coupled equations. For a system consisting of two n-atom isotopic adspecies, one must begin with a set of 6n equations which include the interactions between the active modes of different isotopes. The isotopic coupling strength is usually very strong because of the small frequency difference between the isotopes of interest.

By the concept of the "energy-gap law,"[4] we realize that the interaction strength for a multi-quanta process is relatively weak compared with that of a single-quantum process. Therefore we shall factor out the single-quantum coupling, i.e., the interaction between the active modes of the isotopes, and regard the other all inactive modes of the adspecies and the phonon modes as a heat bath. By this factorization procedure, we have ignored the interactions among the bath modes, although we shall not ignore the bath-mediated coupling between the active modes. Furthermore, the interspecies coupling will be effectively accounted for by an ensemble-averaging procedure.

We first consider the simple system depicted by Fig. 1(A), which consists of only two interacting isotopic adspecies A and B with active mode frequencies ω_A and ω_B, respectively, and both coupled to a common bath C with frequencies ω_j. The total vibrational Hamiltonian of the system may be written as

$$H_1 = H_0 + H_{AB} + H_{ACB} + H_{AC} + H_{BC} + H_{AF} + H_{BF} . \qquad (1)$$

H_0 is the separable portion, H_{AB} and H_{ACB} are the direct and indirect (bath-mediated) couplings of the active modes, respectively, H_{AC} and H_{BC} represent the irreversible relaxation of the active modes A and B

to the bath modes, respectively, and H_{AF} and H_{BF} are the laser interactions with isotopes A and B, respectively.

The direct excitation of the bath modes, H_{CF}, is not included in the above Hamiltonian, since the far off-resonant excitation is significantly weak compared with that of near-resonant excitation, i.e., we shall be interested in a laser radiation with frequency $\omega \approx \omega_A$, ω_B and $\omega >> \omega_j$. Furthermore, electronic excitations of the substrate leading to direct bulk heating are neglected, such as infrared excitation of adspecies on a semiconductor surface which has very small absorption coefficient for $\omega \simeq 1000\sim3000$ cm^{-1}. We note that the bath-mediated interaction Hamiltonian, H_{ACB}, is primarily governed by the intraspecies inactive modes, since the intramolecular anharmonic relaxation (IAR) is usually much faster than that of the phonon relaxation. [Note that the bath (C) modes consist of the inactive modes of the adspecies as well as the phonon modes.] Based on the relative strengths of the pumping rates ($V_{A,B}$), the direct active-mode coupling (D_{AB}), the bath-mediated coupling (D_{ACB}) and the multiphonon relaxation ($D_{A,BC}$), which are governed respectively by the Hamiltonians $H_{A,BF}$, H_{AB}, H_{ACB} and $H_{A,BC}$, we may distinguish several types of excitations: (i) single-mode (A) selective, for $V_A >> V_B$, D_{AB}, D_{ACB}, $D_{A,BC}$; (ii) active-mode (A and B) selective, for $V_A \approx V_B >> D_{AB}$, D_{ACB}, $D_{A,BC}$ or $V_A \approx D_{AB} >> V_B$, D_{ACB}, $D_{A,BC}$; (iii) functional-group selective (or adspecies selective), for $V_A \approx V_B \simeq D_{AB} \simeq D_{ACB} >> D_{A,BC}$, i.e., selective bond breaking is still possible, even when IAR is very fast, if the multiphonon relaxation is considerably weak; and (iv) nonselective thermal heating, for $D_{A,BC} \approx V_{A,B}$, D_{ACB}, D_{AB}.[5]

We now extend the above model to a system consisting of a group of isotopic mixtures, which is represented by Fig. 1(B). Notice that the density of states peaked at ω_A and ω_B are further broadened compared to those in Fig. 1(A) due to the additional interspecies interactions. The total Hamiltonian for this more general system may be written as

$$H_2 = H_1 + H_{AA} + H_{BB} + H_{ACA} + H_{ABA} + H_{BCB} + H_{BAB}, \tag{2}$$

where H_1 is given by Eq.(1), and we have now included the active mode couplings within the same isotope, H_{AA} and H_{BB}, as well as the indirect couplings, $H_{ijk}(i,j,k = A,B,C)$. A more explicit description of the above model system is provided by the second quantization representation of the total Hamiltonian. The unperturbed Hamiltonian for anharmonic isotopes is

$$H_0 = \sum_i \hbar(\omega_A - \varepsilon_A^* a_i^\dagger a_i) a_i^\dagger a_i + \sum_j \hbar(\omega_B - \varepsilon_B^* b_j^\dagger b_j) b_j^\dagger b_j, \tag{3}$$

where each sum runs over all the individual species for a given isotope (A or B with anharmonicity ε_A^* or ε_B^*, respectively). The direct interaction Hamiltonians are given by

$$H_{AB} = \sum_{i,j} \hbar D_{AB} a_i^\dagger b_j + h.c., \tag{4.a}$$

$$H_{AC} = \sum_i \hbar F_{ip}^A C_p a_i^\dagger + h.c., \tag{4.b}$$

$$H_{BC} = \sum_j \hbar F_{jp}^B C_p b_j^\dagger + h.c., \tag{4.c}$$

$$H_{AA} = \sum_{i,k} \hbar D_{AA} a_i^\dagger a_k + h.c., \tag{4.d}$$

$$H_{BB} = \sum_{j,k} \hbar D_{BB} b_j^\dagger b_k + h.c., \tag{4.e}$$

where D and F are the appropriate interaction constants among different modes, $C_p = \prod_\nu c_\nu$ is a multiphonon operator for a p-phonon process and h.c. stands for the Hermitian conjugate.[2] The indirect interaction Hamiltonians can be represented as

$$H_{ACB} = \sum_{i,j} \hbar \prod_\nu G^\nu_{AB} C^\dagger_\nu C_\nu a^\dagger_i b_j + h.c., \tag{5.a}$$

$$H_{ACA} = \sum_{i,k} \hbar \prod_\nu G^\nu_{AA} C^\dagger_\nu C_\nu a^\dagger_i a_k + h.c., \tag{5.b}$$

$$H_{ABA} = \sum_{i,j,k} \hbar K_{AA} b^\dagger_j b_j a^\dagger_i a_k + h.c., \tag{5.c}$$

with similar expressions for H_{BCB} and H_{BAB}. We note that the appropriate indirect coupling constants G and K are constructed by energy conservation such that no energy is transferred from the A mode to the bath (C) modes and the B mode, respectively. Finally, the laser field interaction Hamiltonians are given by

$$H_{AF} = \sum_i \hbar V_A \cos\omega t \, (a^\dagger_i + a_i), \tag{6.a}$$

$$H_{BF} = \sum_j \hbar V_B \cos\omega t \, (b^\dagger_j + b_j), \tag{6.b}$$

$$V_{A,B} = (\hbar/2m_{A,B}\omega_{A,B})^{1/2} \mu'_{A,B}(0) E \cos\theta, \tag{6.c}$$

where $\mu'(0)$ is the derivative of the dipole moment of the pumped-mode evaluated at the equilibrium point, and E is the electric field of the radiation, assumed to be time-independent, with circular frequency ω and linearly polarized at an angle θ with respect to $\mu'(0)$.

III. Equations of Motion in the Heisenberg-Markoffian Picture

To investigate the energy transfer dynamics, i.e., the time evolution of the number of photons absorbed by the isotopes accompanied by bath-induced damping, we shall first set up the equations of motion which involve the many-body effects resulting from both the active modes and the bath modes. For a group of isotopic adspecies subjected to laser radiation, a physical measurement would deal with an ensemble-averaged quantity over both the active and the bath modes coordinates, e.g., the average excitations of the isotopes (photon absorbed per adspecies). Assuming there are n_A and n_B adspecies for isotopes A and B, respectively, then we shall be interested in the average excitations defined by $\langle N_A \rangle \equiv \langle\langle \Sigma_j a_j^\dagger a_j \rangle\rangle / n_A$ and $\langle N_B \rangle \equiv \langle\langle \Sigma_j b_j^\dagger b_j \rangle\rangle / n_B$, where the double bracket $\langle\langle \cdots \rangle\rangle$ denotes the ensemble average (or trace) over both the active and bath modes. The many-body effects due to the coupling between the active and bath modes may be reduced to damping factors either by the Wigner-Weisskopff approximation (WWA) or by the Markoffian approximation.[6] To utilize WWA, one would first take the Laplace transform of the equations of motion and use the so-called "single-pole" approximation to reduce the many-body effects governed by a summation over the bath modes. Here, we shall use the latter approach and set up the equations of motion in the Heisenberg-Markoffian picture (HMP). In HMP no memory effects are retained, which assumes that the correlation time of the bath modes is much shorter than the energy damping time of the active modes such that energy going into the bath will not return to the active modes. The significance of the energy feedback effects on excitations of the active modes will be discussed in Section VII.

Picturing the system in HMP, the equations of motion for the ensemble-averaged excitations of isotopes A and B, denoted by $\langle N_A \rangle$ and $\langle N_B \rangle$, respectively, can be represented as the following set of coupled nonlinear equations derived with the help of Kubo's cumulant expansion:[2,6,7]

$$i\dot{\bar{A}} = \omega_{eff}^{A}(t)\,\bar{A} + \bar{V}_A \cos\omega t + \bar{D}_{AB}\bar{B}, \tag{7.a}$$

$$i\dot{\bar{B}} = \omega_{eff}^{B}(t)\,\bar{B} + \bar{V}_B \cos\omega t + \bar{D}_{AB}\bar{A}, \tag{7.b}$$

$$i\langle \dot{N}_A(t)\rangle = \bar{V}_A \cos\omega t \langle \bar{A}^{\dagger} - \bar{A}\rangle - \bar{D}_{AB}\langle \bar{A}\bar{B}^{\dagger} - \bar{A}^{\dagger}\bar{B}\rangle - i\gamma_1^{A}(\langle N_A\rangle - \bar{n}_c/2), \tag{7.c}$$

$$i\langle \dot{N}_B(t)\rangle = \bar{V}_B \cos\omega t \langle \bar{B}^{\dagger} - \bar{B}\rangle + \bar{D}_{AB}\langle \bar{A}\bar{B}^{\dagger} - \bar{A}^{\dagger}\bar{B}\rangle - i\gamma_1^{B}(\langle N_B\rangle - \bar{n}_c/2), \tag{7.d}$$

$$\langle \omega_{eff}^{A,B}(t)\rangle = \omega_{A,B} - 2\xi_{A,B}^{*}\langle N_{A,B}(t)\rangle - i\Gamma_{A,B}/2, \tag{7.e}$$

$$\Gamma_{A,B} = \gamma_1^{A,B} + \gamma_2^{A,B}, \tag{7.f}$$

$$\bar{n}_c = [\exp(\hbar\bar{\omega}_c/kT) - 1]^{-1}. \tag{7.g}$$

Here we have used the ensemble-averaged quantities $\langle \Sigma_i a_i\rangle/n_A = \bar{A}$, $\langle \Sigma_i a_i^{\dagger} V_A\rangle/n_A \approx \bar{V}_A\bar{A}$, $\langle \Sigma_{i,j} D_{AB} a_i b_j\rangle/(n_A n_B) \approx \bar{D}_{AB}\bar{A}^{\dagger}\bar{B}$, etc.

We note that the ensemble-averaged operators of different active modes are assumed to be uncorrelated, i.e., $\langle a^{\dagger}b\rangle = \langle a^{\dagger}\rangle\langle b\rangle$, since the average quantity $\langle \ldots \rangle$ over the bath-mode coordinates remains an operator in the active-mode coordinates, and their correlation via the surface-induced random force, which is assumed to be a "white" noise, is negligible. We also assume the bath modes to be in thermal equilibrium, and hence the mean occupation number of the bath mode, $\bar{n}_c$, is constant. [The transient behavior with a time-dependent $\bar{n}_c$ caused by substrate heating will be discussed in Section VII.] Moreover, we have used the ansatz $\langle a^{\dagger}aa\rangle \approx \langle a^{\dagger}a\rangle\langle a\rangle$, etc.

The important features of the above equations of motion are: (i) The active modes of the mixed isotopes, with average excitations $\langle N_{A,B}\rangle$, are pumped by laser radiation via $\bar{V}_{A,B}$ and relax to a common bath via the multi-phonon (T_1) energy damping factor $\gamma_1^{A,B}$, where the energy fluctuation

of the bath modes is given by the Bose-Einstein distribution $\bar{n}_c$ with a mean frequency $\bar{\omega}_c$ and evaluated at the surface temperature T; (ii) The reversible energy transfer between the active modes A and B is governed by the mean isotope coupling strength $\bar{D}_{AB}$ [note that the second terms in Eq.(7.c) and in Eq.(7.d) have opposite signs]; (iii) The coupled equations for the excitations $\langle N_A \rangle$ and $\langle N_B \rangle$ are highly nonlinear due to the excitation-dependent effective frequency $\omega_{eff}^{A,B}(t)$ which is complex and time-dependent. [The surface-induced frequency shift of $\omega_{A,B}$ is ignored in Eq.(7.e).] The total width, i.e., the imaginary part of $\omega_{eff}^{A,B}$, is given by the superposition of the energy (T_1) relaxation factor $\gamma_1^{A,B}$ and the phase (T_2) relaxation factor $\gamma_2^{A,B}$. While $\gamma_1^{A,B}$ arises mainly from the direct interaction part of the Hamiltonian, H_{AC} and H_{BC}, the dephasing factor $\gamma_2^{A,B}$ is mainly due to the indirect interactions such as H_{AA}, H_{BB}, H_{ACA}, etc. [For an explicit expression of $\Gamma_{A,B}$, we refer the reader to Ref. 2.] (iv) In the absence of interisotopic coupling, $\bar{D}_{AB} = 0$, active modes A and B are noninteracting and the difference of the excitations $\langle N_A \rangle - \langle N_B \rangle$ will be characterized only by the frequency difference $\omega_{eff}^{A} - \omega_{eff}^{B}$, if $\bar{V}_A = \bar{V}_B$; (v) in the absence of laser radiation, $\bar{V}_{AB} = 0$, the steady-state total excitation $\langle N_A \rangle + \langle N_B \rangle$ goes to the thermal equilibrium value $\bar{n}_c$ as expected from the sum of Eqs.(7.c) and (7.d).

The above coupled equations can also be set up by a phenomenological approach, where active-mode operator $\hat{O} = a^\dagger$, a or $a^\dagger a$ obeys the equation

$$i\frac{d\langle\langle \hat{O} \rangle\rangle}{dt} = \left\{ (\bar{V}_A + D_{AB}) \left\langle\left\langle \frac{d\hat{O}}{dt} \right\rangle\right\rangle + \omega_{eff}^{A} \left\langle\left\langle a^\dagger \frac{\partial \hat{O}}{\partial a^\dagger} \right\rangle\right\rangle + \frac{i\Gamma_A}{2} \left\langle\left\langle \frac{\partial \hat{O}}{\partial a} a \right\rangle\right\rangle + h.c. \right\}$$
$$+ (i\Gamma_A/2)\bar{n}_c \left\langle\left\langle \frac{\partial^2 \hat{O}}{\partial a \partial a^\dagger} \right\rangle\right\rangle + \left\langle\left\langle \frac{d\hat{O}}{dt} \right\rangle\right\rangle_{T_2} . \qquad (8)$$

This dephasing term is mathematically constructed such that for $\hat{O} = a^{\dagger}$ and $a^{\dagger}a$,

$$\left\langle\!\left\langle \frac{da^{\dagger}}{dt} \right\rangle\!\right\rangle_{T_2} = -\gamma_2^{A} \langle\!\langle a^{\dagger} \rangle\!\rangle , \tag{9.a}$$

$$\left\langle\!\left\langle \frac{da^{\dagger}a}{dt} \right\rangle\!\right\rangle_{T_2} = 0 , \tag{9.b}$$

that is,

$$\left\langle\!\left\langle \frac{d\hat{O}}{dt} \right\rangle\!\right\rangle_{T_2} = \gamma_2^{A} \left\langle\!\left\langle [a^{\dagger}a, \hat{O}]a^{\dagger}a - a^{\dagger}a[a^{\dagger}a, \hat{O}] \right\rangle\!\right\rangle . \tag{10}$$

This assures that the dephasing (T_2) process changes only the phase of the pumped-mode [see Eqs.(7a) and (7.b)] without changing its excitations. We note that, in Eqs.(7.d) and (7.e), the excitations are damped by $\gamma_1^{A,B}$ only, with no contribution from $\gamma_2^{A,B}$.

Because of the rapidly oscillating optical frequency, $\omega \simeq 10^{13}$Hz, the size of the time step necessary to follow the evolution of the excitations will be as small as 10^{-14} sec, which implies 10^{5} steps to generate the time-dependent excitation profile up to the range of a nanosecond. A way to overcome this difficulty is that, instead of following the optical frequency, one may use the rotating-wave approximation (RWA) which discards the highly oscillatory terms [$\exp(\pm 2i\omega t)$]. In this way one works on the time-scale given by the inverse of the detuning, which is in the range of several nanoseconds for a detuning of several cm^{-1}. For this purpose, we introduce the transforms

$$\bar{A}(t) = A(t) \exp(-i\omega t) , \tag{11.a}$$

$$\bar{B}(t) = B(t) \exp(-i\omega t) , \tag{11.b}$$

and employing RWA, we simplify Eq.(7) to

$$i\dot{A} = \left(\omega_{eff}^{A}(t) - \omega\right) A + \bar{V}_A/2 + \bar{D}_{AB} B . \tag{12.a}$$

$$i\dot{B} = \left(\omega_{eff}^{B}(t) - \omega\right) B + \bar{V}_B/2 + \bar{D}_{AB} A , \tag{12.b}$$

$$\langle \dot{N}_A \rangle = -\bar{V}_A \, \mathrm{Im}\, A - 2\bar{D}_{AB} \, \mathrm{Im}(AB^{\dagger}) - \gamma_1^A \langle N_A \rangle , \tag{12.c}$$

$$\langle \dot{N}_B \rangle = -\bar{V}_B \, \mathrm{Im}\, B + 2\bar{D}_{AB} \, \mathrm{Im}(AB^{\dagger}) - \gamma_1^B \langle N_B \rangle . \tag{12.d}$$

Im denotes the imaginary part, and we have ignored the bath-mode occupation number $\bar{n}_c$ by assuming an initially cold surface and that coherent laser excitation dominates over incoherent thermal effects.

IV. Average Excitation

The equations of motion in Eq.(12), which are nonlinear due to the excitation-dependent effective frequency $\omega_{eff}^{A,B}(t)$, are in general not analytically solvable, particularly for the case of high excitation and strong isotopic coupling in which perturbation theory breaks down. Exact numerical solutions for the excitation will be presented in the next section, but before that we shall investigate some simpler limiting cases below.

(A) Time-Dependent Excitation - Dephasing Effects

For $\epsilon_{A,B}^{*} = \bar{D}_{AB} = 0$, Eq.(12) can be solved exactly to give the time-dependent average excitation of the active mode A (and a similar expression for the active mode B since A and B are noninteracting):

$$\langle N_A(t) \rangle = X_1 \left\{ 1 - \exp(-\gamma_1^A t) + (\gamma_1^A F/\bar{\Gamma}_A)/(\bar{\Gamma}^2 + \Delta_A^2) \right\}, \tag{13.a}$$

$$X_1 = (\bar{V}_A/2)^2(\Gamma_A/\gamma_1^A)\Big/[\Delta_A^2 + (\Gamma_A/2)^2] \,, \tag{13.b}$$

$$F = (2\Delta_A^2 + \bar{\gamma}\Gamma_A)[e^{-\gamma_1^A t} - e^{-\Gamma_A t/2}\cdot\cos(\Delta_A t)] - 2\gamma_1^A\Delta_A e^{-\Gamma_A t/2}\cdot\sin(\Delta_A t), \tag{13.c}$$

$$\bar{\gamma} = (\gamma_1^A - \gamma_2^A)/2 \,, \quad \Delta_A = \omega_A - \omega \,. \tag{13.d}$$

Setting the dephasing factor γ_2^A equal to zero, we can further reduce the solution to the simple form

$$\langle N_A(t)\rangle = X_2\left\{1 + e^{-\gamma_1^A t} - 2\,e^{-\gamma_1^A t/2}\cdot\cos(\Delta_A t)\right\} , \tag{14.a}$$

$$X_2 = (\bar{V}_A/2)^2\Big/[\Delta_A^2 + (\gamma_1^A/2)^2] \,. \tag{14.b}$$

We note that X_1 and X_2 are the steady-state solutions ($t\to\infty$) for $\gamma_2^A \neq 0$ and $\gamma_2^A = 0$, respectively. This expression can also be obtained by solving Eq.(12.a) with $\varepsilon_A^* = \bar{D}_{AB} = 0$ to get

$$A(t) = \left[(\bar{V}_A/2)\Big/(-\Delta_A + i\gamma_1^A/2)\right]\cdot\left[\exp(-i\Delta_A t - \gamma_1^A t/2) - 1\right] , \tag{15}$$

and the average excitation is then $\langle N_A(t)\rangle = |A(t)|^2$, provided γ_2^A equals zero.

To demonstrate the effects of γ_1^A, γ_2^A and Δ_A on the excitation, in Fig. 2 we plot the three-dimensional excitation profiles in the $(\gamma_1^A, t, \langle N_A\rangle)$ space. Part (A) slows the excitation profile according to Eq.(14), in which the simple exponential decay in time is governed by the damping factor γ_1^A and the oscillatory behavior results from the detuning $\Delta_A \neq 0$. [The excitation profile for $\gamma_2^A = 0$ was shown previously,[3] but for comparison purposes we show it again here,

except that now the plot is a function of $(V_A/2)^2$ instead of the laser intensity.] Parts (B) - (D), which are significantly different from Part (A), show the excitation profiles including the dephasing effects, i.e., $\gamma_2^A \neq 0$. It is seen that γ_2^A not only affects the steady-state excitation solution X_1 ($\simeq X_2\gamma_1^A/\Gamma_A$, for $\Delta_A \ll \gamma_1^A$), but also changes the transient excitation profiles [see Parts (E) and (F)]. For an alternative picture of the dephasing effects on the average excitation, we plot the time evolution of $\langle N_A(t)\rangle$ alone in Fig. 3 for various values of γ_2^A and γ_1^A, such that $\gamma_1^A + \gamma_2^A$ is constant. It is seen that the average excitation oscillates between the envelopes of $[1 + \exp(-\gamma_1^A t)]$ and $[1 - \exp(-\gamma_1^A t)]$ for the case of $\gamma_2^A = 0$ [Part (A)], while it exponentially increases by $[1 - \exp(-\gamma_1^A t)]$ for the case of large γ_2^A [Part (C)].

(B) Steady-State Excitation - Anharmonic Effects

We now consider anharmonic effects by removing the assumption that $\varepsilon_{A,B}^*$ is zero (but still setting $\bar{D}_{A,B}$ equal to zero). For the limiting case of steady-state excitation, Eq.(12) results in a cubic equation for $\langle N_A\rangle$ (and similarly for $\langle N_B\rangle$):

$$X^3 - \left(\frac{\Delta}{\varepsilon^*}\right)X^2 + \left[\left(\frac{\Delta}{2\varepsilon^*}\right)^2 + \left(\frac{\Gamma}{4\varepsilon^*}\right)^2\right]X - \left(\frac{\Gamma}{\gamma_1}\right)\left(\frac{\bar{V}}{4\varepsilon^*}\right)^2 = 0, \qquad (16)$$

where $X \equiv \langle N_A\rangle$ and the subscript A has been dropped, i.e., $\Delta_A = \Delta$, $\varepsilon_A^* = \varepsilon^*$, etc. The behavior of X is nonlinear with respect to $\bar{V}^2$ and exhibits a "bistability" with respect to Δ. Moreover, the optimal detuning Δ^* is red-shifted with respect to that of the harmonic case ($\Delta^* = 0$), which may be seen be rewriting the cubic equation as

$$X = (\bar{V}/2)^2 (\Gamma/\gamma_1) \Big/ \left[(\Delta - 2\varepsilon^* X)^2 + (\Gamma/2)^2 \right], \qquad (17)$$

which upon differentiation and substitution for $\bar{V}$ from Eq.(16) yields

$$\frac{dX}{d\Delta} = \frac{-2X(\Delta - 2\varepsilon^* X)}{\Delta^2 - 4\varepsilon^* X\Delta + 3(\varepsilon^* X)^2 + (\Gamma/2)^2} \cdot \qquad (18)$$

The optimal detuning then occurs at the maximum ($dX/d\Delta = 0$) and is given by $\Delta^* = 2\varepsilon^* X^*$ (note - the single asterisk which was already attached to ε does not signify an optional condition as it does for Δ and X). At the other extreme where $dX/d\Delta \to \infty$, we obtain a quadratic equation for the detuning, whose two roots correspond to a "bistability" in X as a function of Δ. By equating the two roots, we obtain the critical pumping rate $|\bar{V}|^2 = |\bar{V}^*|^2 = \gamma_1 \Gamma^2/(2\varepsilon^*)$, implying that the existence of the bistability is a consequence of the condition $\bar{V} > V^*$. For a fixed laser intensity, which is proportional to $\bar{V}^2$ (or the pumping rate), the bistability criterion may also be stated in terms of the anharmonicity as $\varepsilon^* > \varepsilon^{**} = (\gamma_1/2)(\Gamma/\bar{V})$. This "bistability" feature of the steady-state excitation is shown in Fig. 4. It is seen that when the anharmonicity ε^* is larger than the critical value, ε^{**}, the excitation profile shows the bistable transition from P to Q as the detuning increases, and from R to S as the detuning decreases. We note that the maximum excitation is red-shifted to $\Delta^* > 0$, which is a general property of any nonlinear oscillator with $\varepsilon^* > 0$. A classical analogy of this nonlinear quantum oscillator has been known for some time.[8]

We now investigate another interesting feature of the nonlinear excitation, namely, the rise time of the steady-state excitation

which, to the best of our knowledge, has not been reported in the literature. For this purpose, the time-dependent excitation with $\bar{D}_{AB} = 0$ and $\varepsilon_A^* = 0$ has been numerically solved. Various rise times of the steady-state excitation are shown in Fig. 5, corresponding to different points along the excitation profile (A) in Fig. 4. In Part (A), the time-dependent excitations with short rise times $[\approx 0.2\ (1/\gamma_1^A)]$ are shown for the portion of the profile far from the optimal detuning Δ^*. The excitations with long rise times $[5$ to $40\ (1/\gamma_1^A)]$ for the portion near the optimal value $\Delta^* = 8.0$ are shown in Part(B). The important feature of the nonlinear excitation, as revealed in curves 3 to 19 of Part(B), is that the rise time dramatically increases as we near the "top" of the profile (A) in Fig. 4, i.e., when $\Delta \to \Delta^*$, and when we reach the critical point, i.e., $\Delta = \Delta^* = 8.0$, the rise time virtually goes to infinity. This is to say that it will take a considerably long time for one to excite the active mode to the maximum steady-state value X*, even when optimal detuning is met ($\Delta = \Delta^*$). In Fig. 6, we display the excitation profiles for the case of low damping in which transient excitations go well beyond their steady-state values, resulting from oscillations due to the detuning. Again, these curves show an increase in the rise time as we approach the bistability transition point [see Part (C)].

V. Total Excitation - Role of the Isotopic Coupling Strength

A system of interacting isotopes, $\bar{D}_{AB} \neq 0$, is governed by a set of coupled cubic equations which are not analytically solvable. For tractable results, we shall investigate the low excitation case, i.e., where anharmonicity is negligible, $2\varepsilon_{A,B}^* \langle N_{A,B} \rangle \ll \Gamma_{A,B}/2$.

We shall further simplify the situation by assuming each active mode A and B to be a two-level system with vibration-vibration transfer strength D, where both upper levels are coupled to a common bath with damping factors γ_A and γ_B. The dephasing factors will be ignored. The total vibrational Hamiltonian of the coupled two-level systems is

$$H_3 = H_0 + H_{AF} + H_{BF} \,, \tag{19}$$

where H_0 is the field-free Hamiltonian including the coupling of the active modes, and $H_{A,BF}$ are the laser interaction Hamiltonians. The bath-induced damping factors have been absorbed in H_0, whose matrix representation has the form

$$M_0 = \hbar \begin{pmatrix} \omega_A - i\gamma_A/2 & D \\ D & \omega_B - i\gamma_B/2 \end{pmatrix} . \tag{20}$$

Diagonalization of M_0 gives the eigenenergies

$$\bar{E}_\pm = \frac{1}{2}\left\{ (\bar{E}_1 + \bar{E}_2) \pm \left[(\bar{E}_1 - \bar{E}_2)(\bar{E}_1 - \bar{E}_2) + (2\hbar D)^2 \right]^{1/2} \right\}, \tag{21.a}$$

$$\bar{E}_{1,2} = E_{1,2} - i\hbar\gamma_{A,B}/2 \,, \tag{21.b}$$

$$E_{1,2} = \hbar\omega_{A,B} \,, \tag{21.c}$$

corresponding to the eigenvectors $|+\rangle$ and $|-\rangle$. These eigenvectors are related to the basis set for the matrix of Eq.(20), with eigenenergies $E_{1,2}$, by

$$\begin{pmatrix} |+\rangle \\ |-\rangle \end{pmatrix} = \begin{pmatrix} \sin\theta & \cos\theta \\ \cos\theta & -\sin\theta \end{pmatrix} \begin{pmatrix} |1\rangle \\ |2\rangle \end{pmatrix} , \tag{22.a}$$

where θ is given as

$$\theta = \frac{1}{2}\tan^{-1}\left(\frac{2\hbar D}{\bar{E}_2 - \bar{E}_1}\right). \tag{22.b}$$

We can separate the real and imaginary parts of E_1 by writing

$$E_+ = (E_2 + \delta E) - i(\gamma_B + \delta\gamma)/2\,, \tag{23.a}$$

$$E_- = (E_1 - \delta E) - i(\gamma_A - \delta\gamma)/2\,, \tag{23.b}$$

where the coupling-induced energy shift δE and level broadening $\delta\gamma$ are given by

$$\delta E = (\sqrt{R}\cos\alpha + E_1 - E_2)/2\,, \tag{24.a}$$

$$\delta\gamma = (\sqrt{R}\sin\alpha + \gamma_A - \gamma_B)/2\,, \tag{24.b}$$

$$\alpha = \frac{1}{2}\tan^{-1}(R_2/R_1)\,, \tag{24.c}$$

$$R = (R_1^2 + R_2^2)^{1/2}\,, \tag{24.d}$$

$$R_1 = (E_2 - E_1)^2 + (2\hbar D)^2 - \hbar(\gamma_A - \gamma_B)^2/4\,, \tag{24.e}$$

$$R_2 = \hbar(\gamma_A - \gamma_B)(E_2 - E_1)\,. \tag{24.f}$$

As shown schematically in Fig. 7, E_+ and E_- are blue- and red-shifted, respectively, with respect to the old state energies E_2 and E_1. Furthermore, the lower and upper levels are narrowed and broadened, respectively, by $\delta\gamma$. It is interesting to note that this broadening (narrowing) effect is found only when the initial level widths are unequal, i.e., $\gamma_A \neq \gamma_B$.

We now expand the wavefunction of the total Hamiltonian H_3 in the complete set $\{|0\rangle, |+\rangle, |-\rangle\}$,

$$|\Psi(t)\rangle = C_0|0\rangle + C_-|-\rangle + C_+|+\rangle, \tag{25}$$

where the coefficient amplitudes $C_n(t)$, $n = 0,+,-$, are time dependent due to the time-dependent laser interaction Hamiltonians $H_{AF}(t)$ and $H_{BF}(t)$. Substituting the above expansion into the time-dependent Schrödinger equation and employing the rotating-wave approximation, we obtain the coupled equations of motion

$$2i\dot{C}_0 = VC_- \exp(-i\Delta_- t) + VC_+ \exp(-i\Delta_+ t), \tag{26.a}$$

$$2i\dot{C}_- = VC_0 \exp(i\Delta_- t) - i\gamma_- C_-, \tag{26.b}$$

$$2i\dot{C}_+ = VC_0 \exp(i\Delta_+ t) - i\gamma_+ C_+, \tag{26.c}$$

where the new detunings and damping factors are given by $\Delta_\pm = (E_\pm - \hbar\omega_{B,A})/\hbar$ and $\gamma_\pm = \gamma_{B,A} \pm \delta\gamma$, respectively. Here we have ignored dephasing effects and assumed $V_+ = V_- = V$. Using time-dependent perturbation theory with the initial conditions $C_0(t) \approx C_0(0) = 1$, $C_\pm(0) = 0$, we obtain the transition probabilities or population functions

$$P_\pm(t) = |C_\pm(t)|^2 = \frac{(V/2)^2}{\Delta_\pm^2 + (\gamma_\pm/2)^2}\left[1 + \exp(-\gamma_\pm t) - 2\cos(\Delta_\pm t)\exp(-\gamma_\pm t/2)\right]. \tag{27}$$

Although these correspond to the average excitations described in the previous section, $P_+(t) \neq \langle N_A(t)\rangle$ and $P_-(t) \neq \langle N_B(t)\rangle$ since the states $|\pm\rangle$ are mixtures of $|1\rangle$ and $|2\rangle$. However, the total excitation $\langle N_A\rangle + \langle N_B\rangle$ is identical to the total population $P_+(t) + P_-(t)$ by energy conservation.

To demonstrate the effects of the isotopic coupling strength, D, on the total excitation, we consider the steady-state case $N_+ \equiv X + Y = (P_+ + P_-)_{t\to\infty}$, which is found to be

$$N_+ = \frac{(V/2)^2}{\Delta_-^2 + (\Gamma_-/2)^2} + \frac{(V/2)^2}{\Delta_+^2 + (\Gamma_+/2)^2} \quad . \tag{28}$$

The above expression is simply a superposition of two Lorentzians which are now decoupled in the new basis. The effects of D on the total excitation are embedded in the new detunings $\Delta_\pm$ and the new level broadenings (or damping factors) $\gamma_\pm$. We note that the above total excitation, proportional to the absorption intensity of the adspecies, may be used in a line-shape fitting procedure. However, an actual adspecies spectrum may be further broadened by, e.g., collisional dephasing which is coverage-dependent and/or shifted compared to that of Eq.(28), where only the T_1(energy) broadening and the isotope coupling induced line-shift are included. We suggest that a coverage- or pressure-dependent measurement of the low intensity absorption spectrum would be a good test of the above diagonalization procedure of a two-level physical system.

The effects of the coupling strength and the frequency difference of the isotopes on the steady-state excitation are shown in Fig. 8. It is seen that the peaks of the profiles, located at the uncoupled active-mode frequencies ω_A and ω_B, are shifted apart for $D \neq 0$ [see Part (A)]. Moreover, the total excitation profiles are governed by the frequency difference, $\omega_A - \omega_B$, and the damping factors $\gamma_{A,B}$. For a small damping factor we expect a high excitation [compare Parts (B) and (C)], and for a small frequency difference we expect a strong interference [compare Parts (C) and (D)]. This red (blue) shift and narrowing (broadening) features can be more easily visualized by the expression of

the total excitation [Eq.(28)], defined in the new basis $|\pm\rangle$ with two decoupled Lorentzians, than in the old basis $\{|1\rangle,|2\rangle\}$ where N_+ is given by a complicated expression in terms of D, $\gamma_{A,B}$ and $\Delta_{A,B}$.[3]

VI. Isotopic Selectivity

In this section we shall investigate the effects of the isotopic coupling strength, the frequency difference and the anharmonicity on the selectivity of isotope separation. Some tractable results for the harmonic case ($\varepsilon^* = 0$) will be analyzed, and then numerical results for more general cases with $\varepsilon^*, D \neq 0$ will be shown graphically. Isotopic selectivity may be visualized in a simple way through the steady-state excitation difference $N_- \equiv X - Y$, where X and Y are the steady-state excitations of the active mode A and B, respectively, which are found from Eq.(12), for $\varepsilon^*_{A,B} = 0$, $V_A = V_B = V$, $\gamma_1^A = \gamma_2^B = \gamma_1$ and $\Gamma_A = \Gamma_B = \Gamma$, to be

$$N_- = V^2 \Gamma \Omega_- (\Omega_+ - 2D) / [4\gamma_1 (Z_1^2 + Z_2^2)], \tag{29.a}$$

$$Z_1 = \Delta_A \Delta_B - D^2 - (\Gamma/2)^2, \tag{29.b}$$

$$Z_2 = \Gamma \Omega_+ / 2, \tag{29.c}$$

$$\Omega_\pm = \Delta_B \pm \Delta_A, \tag{29.d}$$

where $\Delta_{A,B}$ is the detuning and $D \equiv \bar{D}_{AB}$ is the mean isotopic coupling strength.[3]

The above formulas display some important features of laser-stimulated isotope separation: (i) the isotopic selectivity, governed

by the difference excitation N_-, increases when the coupling strength, D, decreases; (ii) for very strong coupling with $D = D^* = \Omega_+/2$, there is zero selectivity, i.e., $N_- = 0$. These coupling-induced interference effects that "smear out" the selectivity of an isotope mixture, which is highly separable if it is weakly coupled, may be visualized more easily by rewriting Eq.(12.a) as

$$i\dot{A} = (\Omega^A_{eff} - \omega) A + \bar{V}_A/2 \ , \tag{30}$$

where the effects of the coupling strength are absorbed in the complex effective frequency $\Omega^A_{eff} = \omega^A_{eff} + DB/A$. This frequency reflects the fact that the coupling term DB/A plays a "frequency-resonance" role in the selective excitation processes, i.e., a strong coupling strength between the isotopic species may reduce the selectivity by "promoting" the isotopic species to a virtually equal frequency level. Moreover, for $D > \Omega_+/2$, N_- may even reverse its sign so that $X < Y$. In the zeroth-order solutions of the equations of motion, i.e., with $D = 0$ in Eq.(12), the active modes of the isotopes are isolated from each other and are independently excited. In this situation, the isotopic selectivity is characterized by their frequency difference, resulting in different absorption cross sections given by

$$\sigma_{A,B} = \frac{(\bar{V}_{A,B}/2)^2 (\Gamma_{A,B}/\gamma_t^{A,B})}{(\omega^{A,B}_{eff} - \omega)^2 + (\Gamma_{A,B}/2)^2} \ . \tag{31}$$

To demonstrate the effects of the coupling strength on both the dynamics and the steady-state excitations, we plot the numerical solutions of Eq.(12) for the harmonic case ($\epsilon^*_{A,B} = 0$) in

Fig. 9. It is seen that $\langle N_A \rangle$ is higher than $\langle N_B \rangle$ for $\Delta_A < \Delta_B$ with D = 0 [Part(A)]. As D increases, both excitations decrease [Part(B)]. Increasing further the coupling strength to the transition value, i.e., D = D*, we see that the steady-state excitations become identical, as expected from Eq.(29). However, the transient excitations at this point are not identical [Part(C)]. For large coupling strength, D > D*, both excitations are low and $\langle N_B \rangle$ is higher than $\langle N_A \rangle$, as expected from Eq.(29) where $N_- < 0$ [Part(D)].

In Fig. 10, we include the anharmonicity ($\varepsilon^*_{A,B} \neq 0$) and plot numerical solutions of Eq.(12). Here the increase of D does not necessarily result in the decrease of $\langle N_A \rangle$ due to the nonlinear behavior of the excitation and the fact that the D induces a frequency shift as seen in the previous section. There turns out to be an optimal set of values (D,ε*) which yield a maximum excitation. For the case shown in Fig. 10 with $(\varepsilon^*_A, \gamma_1^A, \gamma_2^A, \bar{V}_A, \Delta_A, \Delta_B)$ = (1,2,2,10,8.3,5), D ≃ 2.9 is the optimal strength [compare Parts (C) and (D)].

A more realistic investigation of the isotopic selectivity should account for the laser pulse duration, t_p, and for this purpose we can define the isotopic selectivity S by

$$S(t_p) = \frac{\int_0^{t_p} [W_A(t)/m_A(t)] \langle N_A(t) \rangle dt}{\int_0^{t_p} [W_B(t)/m_B(t)] \langle N_B(t) \rangle dt} , \qquad (32)$$

where $W_{A,B}(t)$ is the instantaneous probability rate of transition from $\langle N_{A,B}(t) \rangle$ to the energy range from which dissociation (or desorption) takes place, and $m_{A,B}$ is the initial concentration of the isotopes. For low dissociation (or desorption) yields, $m_{A,B}(t)$

can be taken as constant. By further assuming mean transition rates $\bar{W}_{A,B}$ independent of time, we can define a reduced selectivity $\bar{S} = [\bar{W}_B m_A/(\bar{W}_A m_B)]S$ by

$$\bar{S}(t_p) = \int_0^{t_p} \langle N_A(t)\rangle dt \Big/ \int_0^{t_p} \langle N_B(t)\rangle dt \quad . \tag{33}$$

Solving Eq.(12) numerically, we plot the time evolution of the reduced selectivity in Fig. 11 for some cases of $D = 0$ and Fig. 12 for $D \neq 0$. From Fig. 11 , we see the following features: (i) for the harmonic case, with $\varepsilon^*_{A,B} = 0$, $\bar{S} = 1$ for $\Delta_A = |\Delta_B|$, since the excitations are symmetric with respect to the $\Delta_{A,B} = 0$ axis [Part(E)]; (ii) for $\varepsilon^*_{A,B} \neq 0$, a higher selectivity is shown in Part(B) compared to that of Part(E), due to the nonlinear feature of the excitation [see the profile (A) in Fig. 4] (iii) the nonlinear anharmonic effects on the selectivity are further shown in Part(A),(C) and (D). Depending on the on the portion of the profile (A) in Fig. 4, the effects of the frequency difference, $\Delta_B - \Delta_A$, on the isotope selectivity could be significantly enhanced [compare Part(A) and (D), where in both cases $|\Delta_B - \Delta_A| = 5$].

Fig. 12 reveals the following features: (i) Part(E) shows the effects of D on the selectivity for the case of $\varepsilon^*_{A,B} = 0$ at $D = D^* = (\Delta_A + \Delta_B)/2$, where $\bar{S} = 1$ at steady-state as expected from Eq.(29); (ii) for $\varepsilon^*_{A,B} \neq 0$, D* is "blue-shifted" toward $\bar{S} = 1$ [Part(F)]; (iii) an increase in D shows a decrease in $\bar{S}$ [Parts(A) to (G)], and $\bar{S} < 1$ when $D > D^*$, corresponding to the situation of $\langle N_A\rangle < \langle N_B\rangle$ [see Part(D) of Fig. 9].

Based on the results displayed in Figs.(11) and (12), we conclude that: (i) for low excitation ($\varepsilon^*_{A,B} \approx 0$) and weak isotopic

coupling ($D \simeq 0$), the optimal condition for high selectivity is that the laser frequency should be tuned such that $\Delta_A \simeq 0$ and $\Delta_B > 0$ in order to separate say, A, from B; (ii) for high excitations, anharmonic effects play an important role, with an optimal detuning $\Delta_A = \Delta^* = 2\varepsilon_A^* X$ which may be further "red-shifted" due to the effects of the isotopic coupling strength D. We finally note that the parameters - detunings($\Delta_{A,B}$), frequency difference ($\omega_B - \omega_A$), coupling strength (D) and the laser pumping constant ($\bar{V}_{A,B}$) ranging from 1 to 10 - were chosen to explore the role of anharmonicity and isotopic coupling strength for an unspecified system. However, one should be able to treat a specific system by identifying these parameters with actual physical quantities.

VII. Effects of Energy Feedback from the Heated Substrate

As mentioned in Section II, for infrared excitation, direct vibrational excitations of low-frequency substrate phonon modes are negligible due to large detunings. Direct electronic excitations of the substrate are also negligible in the present model. For example, for a semiconductor with a band gap energy of ~10,000 cm^{-1}, which is much larger than the CO_2 infrared frequency of ~2,000 cm^{-1}, the absorption coefficient is very small. However, indirect heating of the substrate via multiphonon coupling may provide a source of energy feedback which causes thermal-phonon-activated excitation of the active mode.

In this Section, we shall investigate the energy feedback effects on the excitation of the active mode by combining the quantum excitation equation, Eq.(7), and a classical heat diffusion equation to account for the rise of the substrate temperature. To describe the energy transfer between the laser radiation and the system with the subsequence of substrate heating, we shall use the following coupled equations for the average excitation of the active mode (N_1) and of the effective bath mode (N_2):

$$\frac{dN_1}{dt} = \frac{\sigma I}{\hbar\omega} - \gamma(N_1-N_2), \tag{34}$$

$$\frac{dN_2}{dt} = \nabla\cdot[D\nabla N] + \gamma(N_1-N_2). \tag{35}$$

In Eq.(34), the first term is the total pumping rate with absorption cross section σ, laser intensity I and frequency ω. The second term describes the energy relaxation of the active mode with a multiphonon

relaxation rate γ; the energy feedback effect is governed by the difference of the active-mode and bath-mode excitations N_1-N_2. The time-dependent excitation of the bath mode $N_2(t)$ provides the phonon-activated excitation of the active mode. Eq.(35) is simply an energy diffusion equation for the substrate with diffusivity D, with the gradient operator ∇ defined in the direction of the energy flow of the bath mode.

We note that, without the diffusion term, Eq.(34) may be readily derived from Eq.(7) with $N_1 = N_A + N_B$ and replacing the steady-state excitation $\bar{n}_c$ by a time-dependent bath-mode excitation $N_2(t)$. As we shall see, Eq.(7) represents the diffusion limit of Eqs.(34) and (35).

In general, the above coupled equations can only be solved numerically since σ is excitation dependent [see Eq.(31)], D is temperature dependent and I is time dependent, e.g., a gaussian pulse $I(t) = I_0 \exp[-(t/t_p)^2]$. For simplicity, however, we consider a square pulse excitation in the adiabatic limit with a small diffusion length, $\sqrt{Dt}$, and also in the diffusion limit with a large diffusion length of the heated substrate. Moreover, we shall consider the optimal excitation, i.e., the absorption cross section, σ, to be independent of the excitation in order to eliminate the nonlinear coupling in Eq.(34).

In the adiabatic limit, which is a situation of a local heating (via multiphonon coupling) of the substrate surface with a small diffusion length, we may neglect the diffusion term in Eq.(35). The coupled equations can then be solved analytically

to give the reduced excitations (in units of the total excitation, $I_0 t_p \sigma/h\omega$) for the active mode (N_1^*) and the bath mode (N_2^*):

$$N_1^*(t) = [t+f(t)]/2t_p \qquad (36.a)$$

$$N_2^*(t) = [t-f(t)]/2t_p \qquad (36.b)$$

for $0 \leq t \leq t_p$, and

$$N_1^*(t) = [t_p+f(t_p)\exp(-2\gamma t)]/2t_p \qquad (36.c)$$

$$N_2^*(t) = [t_p-f(t_p)\exp(-2\gamma t)]/2t_p \qquad (36.d)$$

for $t \geq t_p$, where $f(t) = [1-\exp(-2\gamma t)]/(2\gamma)$, and t_p is the duration of a square pulse laser with intensity I_0.

On the other hand, in the diffusion limit, the bath-mode energy rapidly diffuses into the bulk of the substrate which behaves like an infinite heat sink. In this case the rise of the substrate surface temperature is not significant, and no energy feedback will be found. The reduced excitations of the active mode may then be well-approximated by

$$N_1^*(t) = (1+N_0^*)[1-\exp(-\gamma t)] \qquad (37.a)$$

for $0 \leq t \leq t_p$, and

$$N_1^*(t) = N_0^*[1-\exp(-\gamma t)] + [\exp(\gamma t_p)-1]\exp(-\gamma t) \qquad (37.b)$$

for $t \geq t_p$, where N_0^* is the steady-state value.

The time evolution of the reduced excitations is shown in Fig. 13 for the adiabatic and diffusion limit. It is seen that

in the adiabatic limit the active mode has a higher excitation than in the diffusion limit, and both N_1^* and N_2^* reach a "quasi" steady-state value of 0.5, for $t \approx 5\ t_p$. We note that long time behavior of both N_1^* and N_2^* is characterized by the diffusion processes even for the small diffusion length case, and in the region of $t >> t_p$ the excitations will exponentially decay to the steady-state value N_0^*. We also see from Fig. 13 that the active-mode excitation $N_1^*(t)$ for the diffusion limit is upshifted to that of the adiabatic limit via the energy feedback provided by the bath-mode excitation, $N_2^*(t)$, which characterizes the local heating of the substrate surface.

The nonequilibrium transient excitations may be viewed in terms of the effective vibrational temperatures which are related to the excitation energy by[5,9]

$$\bar{n}_1 \hbar\omega_1 = N_1 \hbar\omega, \tag{38.a}$$

$$\bar{n}_2 \hbar\omega_2 = N_2 \hbar\omega. \tag{38.b}$$

$\bar{n}_1$ and $\bar{n}_2$ are the average occupation numbers for the active mode and bath mode, respectively, given by the Bose-Einstein distribution

$$\bar{n}_{1,2}(t) = [\exp(\hbar\omega_{1,2}/kT_{1,2}^{eff}) - 1]^{-1}, \tag{39}$$

where ω_1 and ω_2 are the mean frequency of the active and bath mode, respectively, and the transient effective temperatures T_1^{eff} and T_2^{eff} are for the active and bath mode, respectively. By this

concept of transient temperatures, which are governed by the transient excitations, one may selectively excite the active mode in terms of a high pumping rate for a system with a slow relaxation rate and a small diffusion length. In the transient region, as shown in Fig. 13, the excitations $N_1^*(t) > N_2^*(t)$ give us a higher transient effective temperature of the active mode compared to that of the bath mode, i.e., $T_1^{eff} > T_2^{eff}$.

As discussed in the previous Section, the isotope selectivity characterized mainly by the absorption cross sections of the isotope [Eq.(31)] is strongly frequency dependent due to coherent laser excitation. The incoherent thermal excitations of the active modes due to the energy feedback of the heated substrate, which is frequency independent, would smear out part of the isotope selectivity, which is governed by the ratio N_A/N_B, although the energy feedback causes a higher total excitation $N_1 \equiv N_A + N_B$. We finally propose that for the improvement of the laser-stimulated isotopic separation, one may minimize the energy feedback effects by using an initially cold substrate or using high diffisivity materials to reduce the local surface heating.

VIII. Conclusion

In the present paper, the nonlinear effects of laser-excited anharmonic interacting isotopes and the effects of the isotopic coupling strength, the energy (T_1) and phase (T_2) relaxation rates and the frequency difference on the average excitations are theoretically investigated. The important features are summarized as follows:

(i) The average excitations of interacting isotopes are governed by a set of coupled equations [Eq.(7)], where the anharmonic quantum oscillators coupled to the bath modes are described by the effective frequency $\omega_{eff}^{A,B}$ which is complex and time dependent

due to the anharmonic correction $2\varepsilon^*_{A,B}\langle N_{A,B}(t)\rangle$ and the overall level width $\Gamma_{A,B} = \gamma_1^{A,B} + \gamma_2^{A,B}$.

(ii) The time-dependent average excitation is given by a complicated expression [Eq.(13)] which reduces to a simple Lorentzian for the case of $\gamma_2 = D = 0$.

(iii) For high excitation, the anharmonic correction is significant, and the steady-state excitation is governed by a cubic equation with a "bistability" and a red-shifted optimal detuning [Eq.(16)]. The rise time of the nonlinear excitation dramatically increases as the "trajectory" approaches the optimal value Δ^* [Figs. 5 and 6].

(iv) The adspecies spectrum associated with the total steady-state excitation and characterized by the coupling strength, the frequency difference and the level widths of the isotopes is found to be a superposition of two Lorentzians which are completely decoupled by a diagonalization procedure [Eq.(28)].

(v) The steady-state excitation difference N_-, for a low excitation with $\varepsilon^*_{A,B} = 0$, is characterized by a critical coupling strength $D^* = \Omega_+/2$ [Eq.(29)]. For a high excitation but with weak coupling, $\varepsilon^*_{A,B} \neq 0$, $D \approx 0$, the isotopic selectivity depends on the absorption cross sections of the isotopes in which the frequency $\omega_{eff}^{A,B}$ plays the essential role [Eq.(31)]. For a strong coupling case, $D > 0$, the reduced selectivity is found numerically [Eq.(33)]. The results shown in Figs. 11 and 12 suggest that high isotopic selectivity may be achieved by tuning the laser frequency to an optimal value which is red-shifted with respect to that of the noninteracting case, i.e., $D = 0$, given by $\Delta^* = 2\varepsilon^* X$.

Acknowledgments

This work was supported in part by the Office of Naval Research and the Air Force Office of Scientific Research (AFSC), United States Air Force, under Grant AFOSR-82-0046. The United States Government is authorized to reproduce and distribute reprints for governmental purposes notwithstanding any copyright notation hereon. TFG acknowledges the Camille and Henry Dreyfus Foundation for a Teacher-Scholar Award (1975-82).

*Also affiliated with the Laboratory for Laser Energetics, University of Rochester, NY 14620 USA

References

1. Multiphoton Processes, eds. J. H. Eberly and F. Lambropoulos (Wiley, New York, 1978); Special Issue on Laser Chemistry, Phys. Today 33 (11), 25-59 (1980).
2. J. Lin, A. C. Beri, M. Hutchinson, W. C. Murphy and T. F. George, Phys. Lett. 79A, 233 (1980).
3. J. Lin and T. F. George, unpublished.
4. A. Nitzan and J. Jortner, Mol. Phys. 25, 713 (1973); A. Nitzen, S. Mukamel and J. Jortner, J. Chem. Phys. 60, 3929 (1974).
5. J. Lin and T. F. George, J. Phys. Chem. 84, 2957 (1980); Surface Sci. 108, 340 (1981).
6. W. H. Louisell, Quantum Statistical Properties of Radiation (Wiley, New York, 1973).
7. R. Kubo, in: Fluctuation, Relaxation and Resonances in Magnetic Systems, ed. D. ter Haar (Oliver and Boyd, Edinburgh, 1962).
8. N. N. Bogoliubov and Y. A. Mitropolsky, Asymptotic Methods in the Theory of Non-linear Oscillators (Gordon and Breach, New York, 1961).
9. J. Lin and T. F. George, J. Chem. Phys. 72, 2554 (1980).

Figure Captions

Figure 1. Schematic diagrams of the density of states and the interactions among the A, B and C modes described by the Hamiltonians $H_1(A)$ and $H_2(B)$.

Figure 2. Excitation profiles in $(\gamma_1^A, t, \langle N_A \rangle)$ space for $(\Delta_A, \bar{V}_A) = (5,5)$ and the ratio γ_2^A/γ_1^A = (A)0, (B)1, (C)3, and (D)10. Parts(E) and (F) represent different viewing angles of Parts(A) and (D), respectively, and show the effects of the dephasing factor γ_2^A on the transient excitations. The values of the points P_1 and P_2 are (0.05,0,0) and $(4.25,6,X_1)$, respectively, where X_1 is the steady-state excitation.

Figure 3. Time evolution of the average excitation for $(\varepsilon_A^*, \bar{V}_A, \Delta_A) = (0,10,5)$ and (γ_1^A, γ_2^A) = (A)(2,0), (B)(1,1) and (C)(0.2,1.8). Note that $\gamma_1^A + \gamma_2^A$ remains constant.

Figure 4. Anharmonic steady-state excitations showing the bistability feature for $(\gamma_1, \gamma_2, \bar{V})$ = (4,4,10) and (A) at the critical value of $\varepsilon^* = \varepsilon^{**} = 1.28$ and (B) above the critical value, $\varepsilon^* = 2.56 > \varepsilon^{**}$. The bistable points are shown by P,Q,R and S. The harmonic steady-state excitation (dotted curve) is a Lorentzian.

Figure 5. Time evolution of the average excitation for high damping cases, $\gamma_1 = \gamma_2 = 4$ and $\bar{V} = 10$. In Part(A), $(\varepsilon^*,\Delta) = (0,0)$, $(\varepsilon^{**},7.9)$, $(\varepsilon^{**},\Delta^*)$, $(\varepsilon^{**},8.1)$, $(\varepsilon^{**},-5)$ and $(0,7.9)$ for curves 1,2,3,4,5 and 6, respectively. In Part(B), $\varepsilon^* = \varepsilon^{**}$, $\Delta = 7.8$ (curve 1), 7.9 (curve 2) and $\Delta = 7.968 + 0.002n$, $n = 1,15$ for curves 3 to 17, respectively, $\Delta = 7.999$ (curve 18), $\Delta = 7.9995$ (curve 19), $\Delta = \Delta^*$ (curve 20), $\Delta = 10$ (curve 21) and $\Delta = 12$ (curve 22). Note that $(\varepsilon^{**},\Delta^*) = (1.28,8.0)$ are the optimal values which give a maximal steady-state excitation $X^* = 3.125$.

Figure 6. Time evolution of the average excitation for a case of low damping with $\gamma_1 = \gamma_2 = 2$, $\bar{V} = 10$ and $\varepsilon^* = 1$. In Part(A), the detuning $\Delta = -5,0,5,8.3,8.4$ and 10 for curves 1 to 6, respectively. In Part(B), $\Delta = 8.7$ (curve 1), 8.72 (curve 2), $\Delta = 8.738 + 0.02n$, $n = 1,4$ for curves 3 to 7, respectively, and $\Delta = 8.749$ (curve 8).

Figure 7. Schematic energy diagram for the interacting active modes with energies E_1 and E_2, respectively, coupled to each other by D and excited by the pumping rate V. The coupled basis $\{|1>,|2>\}$ is transformed to a new basis $\{|+>,|->\}$ where the energy is red(blue) shifted by δE and broadened(narrowed) by $\delta\gamma$.

Figure 8. Total excitation profiles in $(N_+, \omega_{A,B}, D)$ space for $\varepsilon^* = 0$, $\gamma_2^{A,B} = 0$, $V = 10$ and $(\omega_B - \omega_A, \gamma_A, \gamma_B)$ = (A)(15,5,5), (B)(15,7,3), (C)(15,3,7) and (D)(5,3,7).

Figure 9. Time-dependent excitations, $\langle N_{A,B}(t) \rangle$, of the active modes for the harmonic case, i.e., $\varepsilon^* = 0$ with $(V, \gamma, \Delta_A, \Delta_B) = (10,1,4,8)$ and D = (A)0, (B)2, (C)D* and (D)10. $D^* = (\Delta_A + \Delta_B)/2 = 6$ is the transition value where $N_- = 0$.

Figure 10. Time evolution of $\langle N_A \rangle$ for the anharmonic case with $\varepsilon^* = 1$, $(V, \gamma, \Delta_A, \Delta_B) = (10,2,8.3,5)$ and D = (A)0, (B)1, (C)2.9 and (D)2.95.

Figure 11. Time evolution of the reduced selectivity [Eq.(33)] for some cases of D = 0: $(\gamma_1^{A,B}, \gamma_2^{A,B}, V) = (4,4,10)$ and $(\varepsilon^*, \Delta_A, \Delta_B)$ = (A)(1.28,5,10), (B)(1.28,5,-5), (C)(0,5,10), (D)(1.28,5,0) and (E)(0,5,-5).

Figure 12. Same as Fig. 11 but for the cases of D = 0 and $D \neq 0$ with $(\varepsilon^*, \gamma_1^{A,B}, \gamma_2^{A,B}, \Delta_A, \Delta_B, V) = (1.28,4,4,5,10,10)$ and D = (A)0, (B)2, (C)4, (D)6, (F)D* and (G)10. Part(E) shows the harmonic case $(\varepsilon^*, D) = (0, D^*)$, where $D^* = (\Delta_A + \Delta_B)/2$ is the transition value.

Figure 13. Time evolution of the reduced excitations (in units of $I_0 t_p \sigma/h\omega$) generated by a square pulse of intensity I_0 and width t_p, for the active mode, N_1^* (solid curve), and the bath-mode, N_2^* (dashed curve) in the adiabatic limit and for the active mode in the diffusion limit (dotted curve). The total reduced excitation is shown by the dashed-dotted line. Here a relaxation rate $\lambda = 0.5/t_p$ is used.

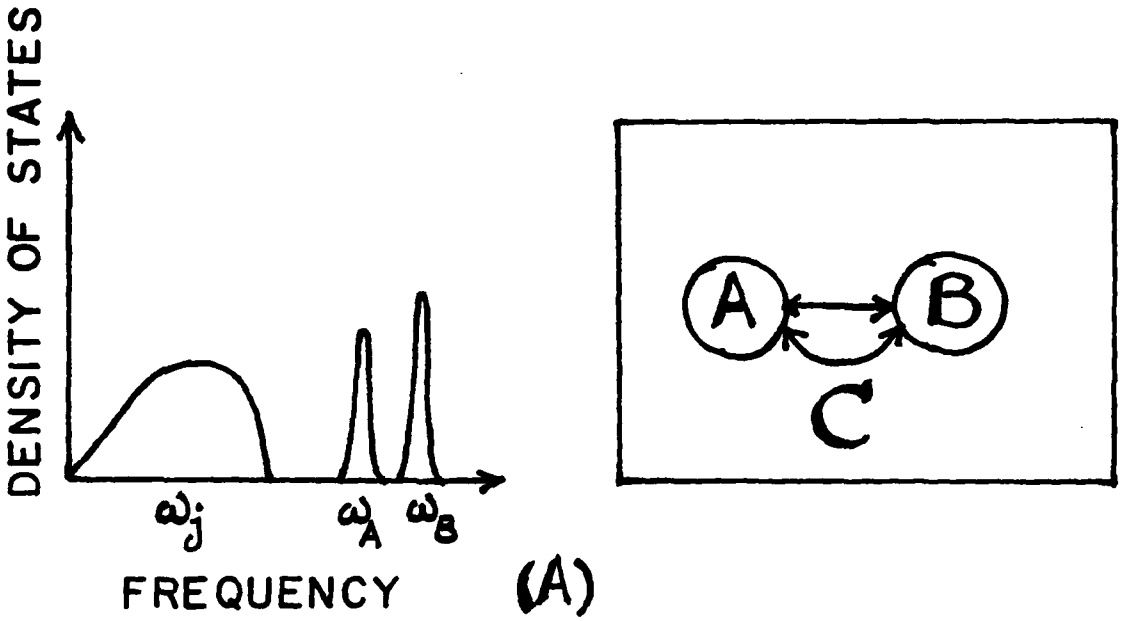

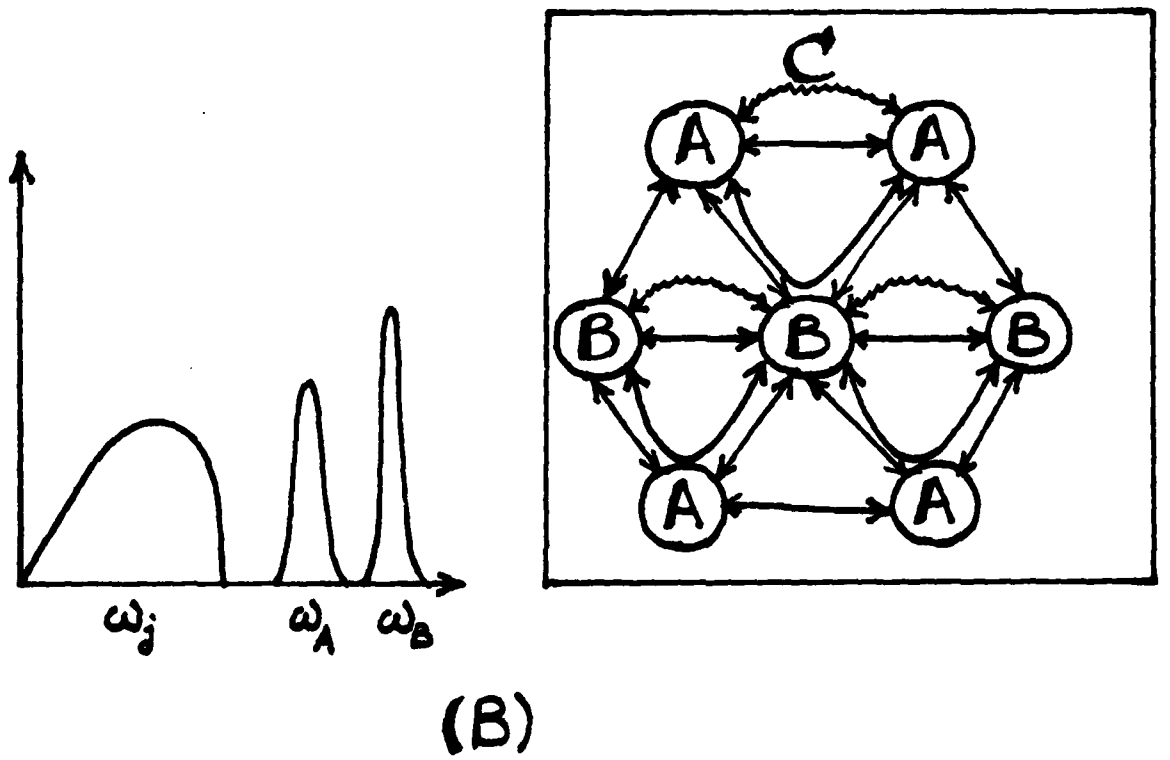

Fig 1. (A) & (B)

Lin & Gregg

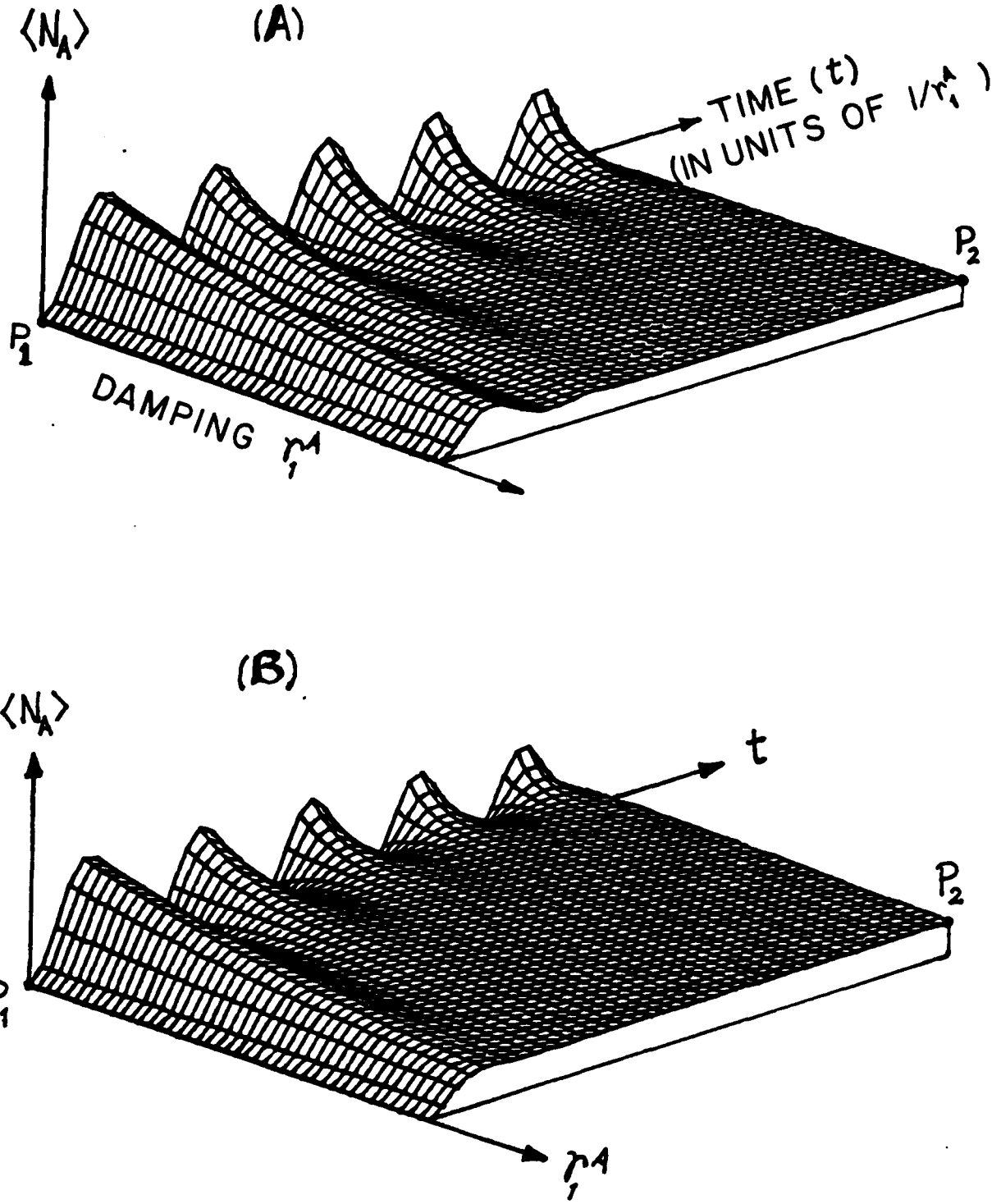

Fig. 2

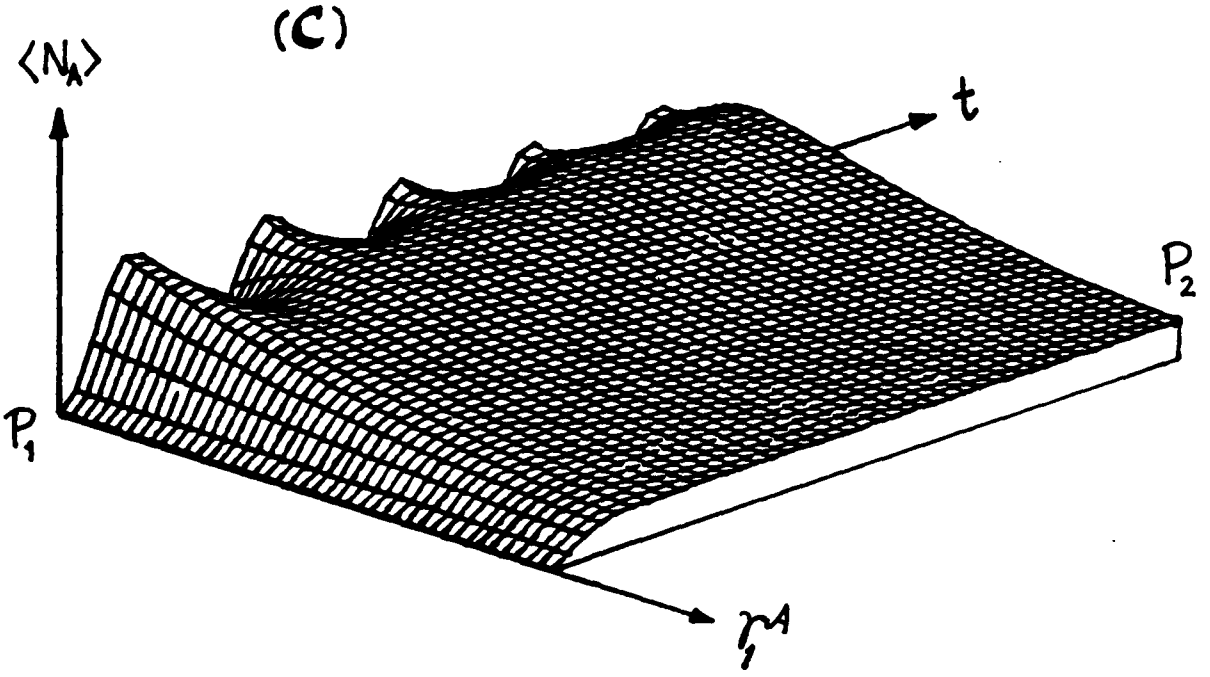

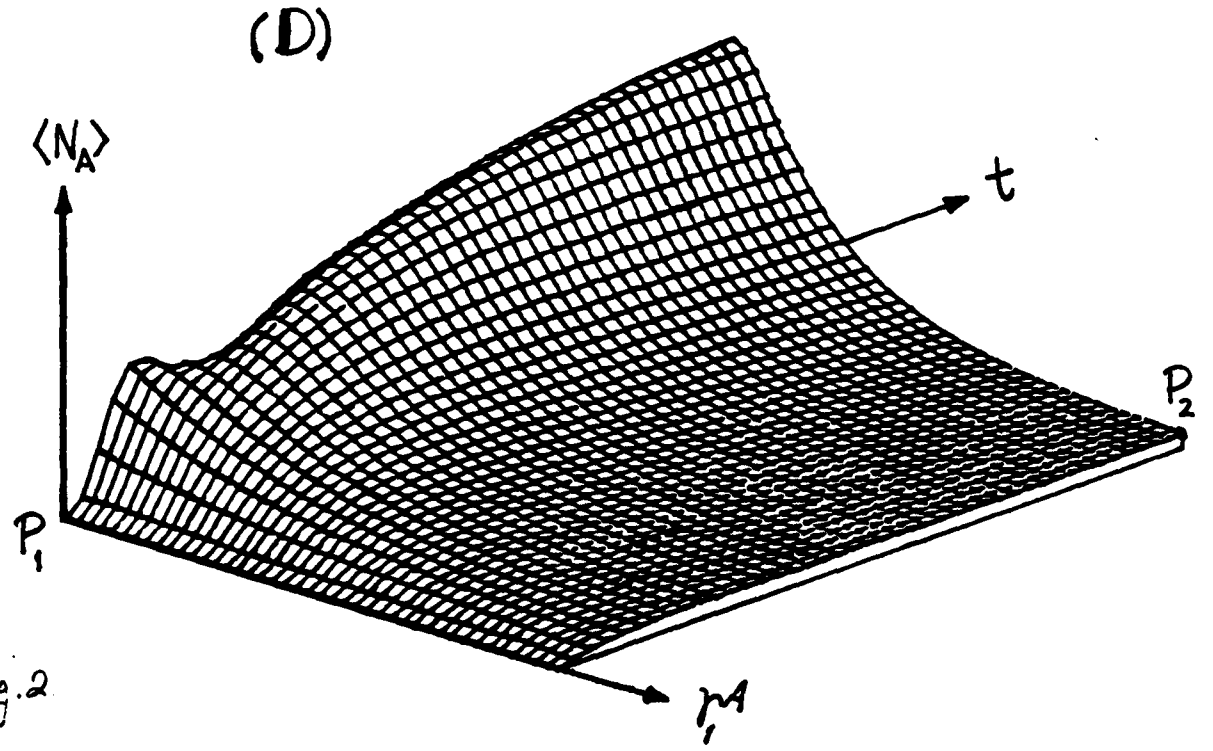

Fig. 2

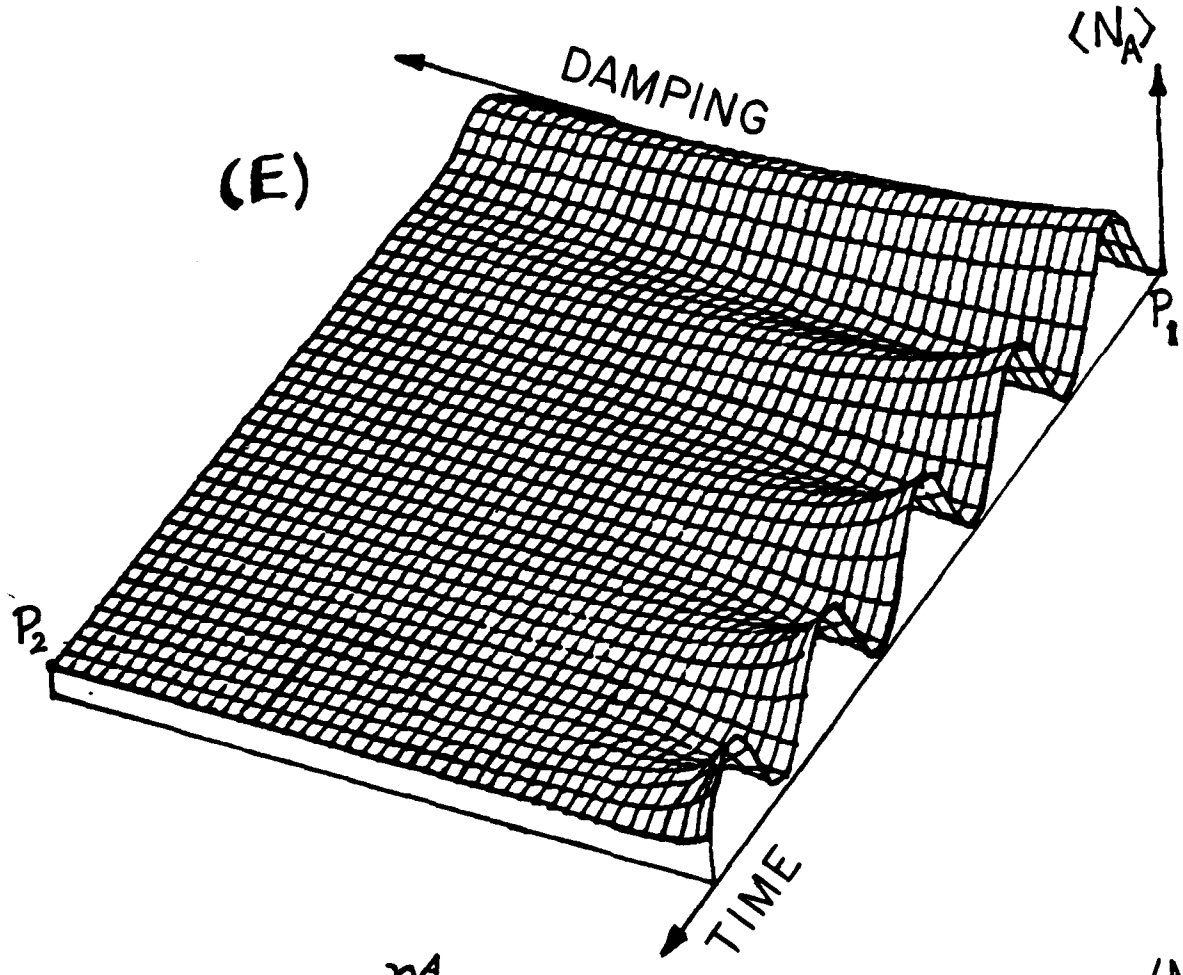
(E)
DAMPING
$\langle N_A \rangle$
P_1
P_2
TIME

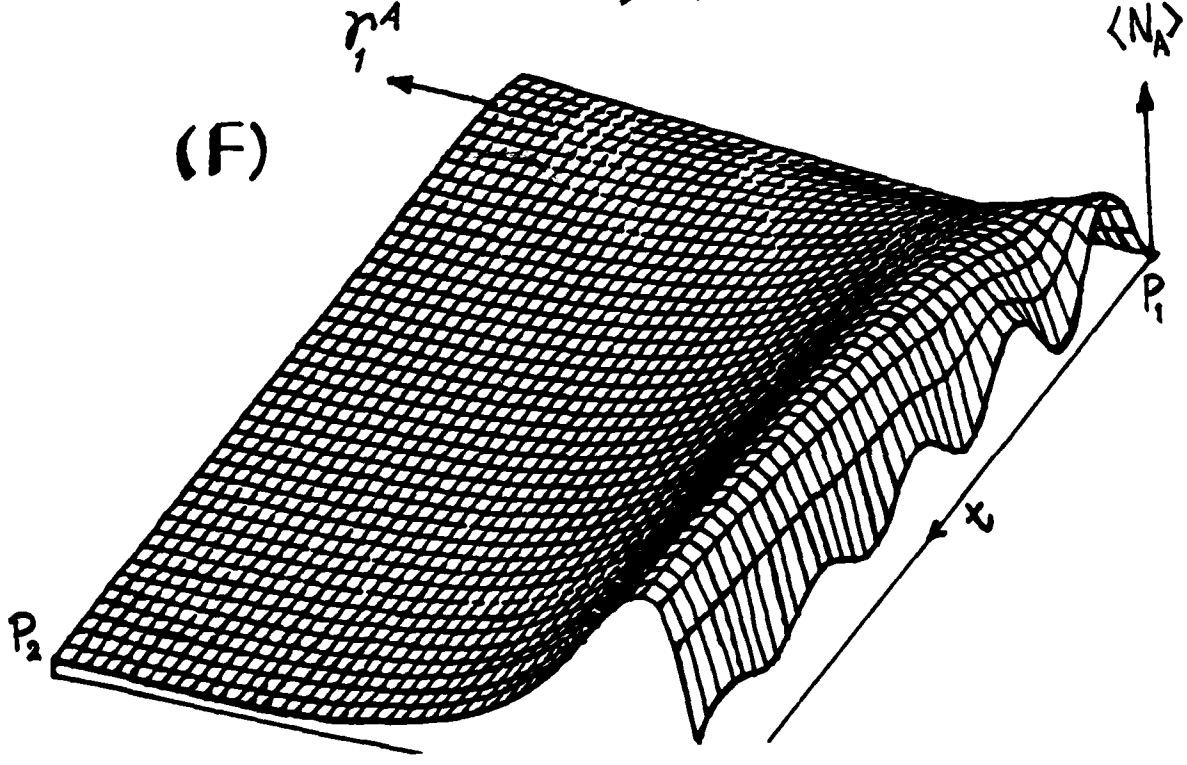
(F)
γ_1^A
$\langle N_A \rangle$
P_1
P_2
t

Fig 2

Fig 2.

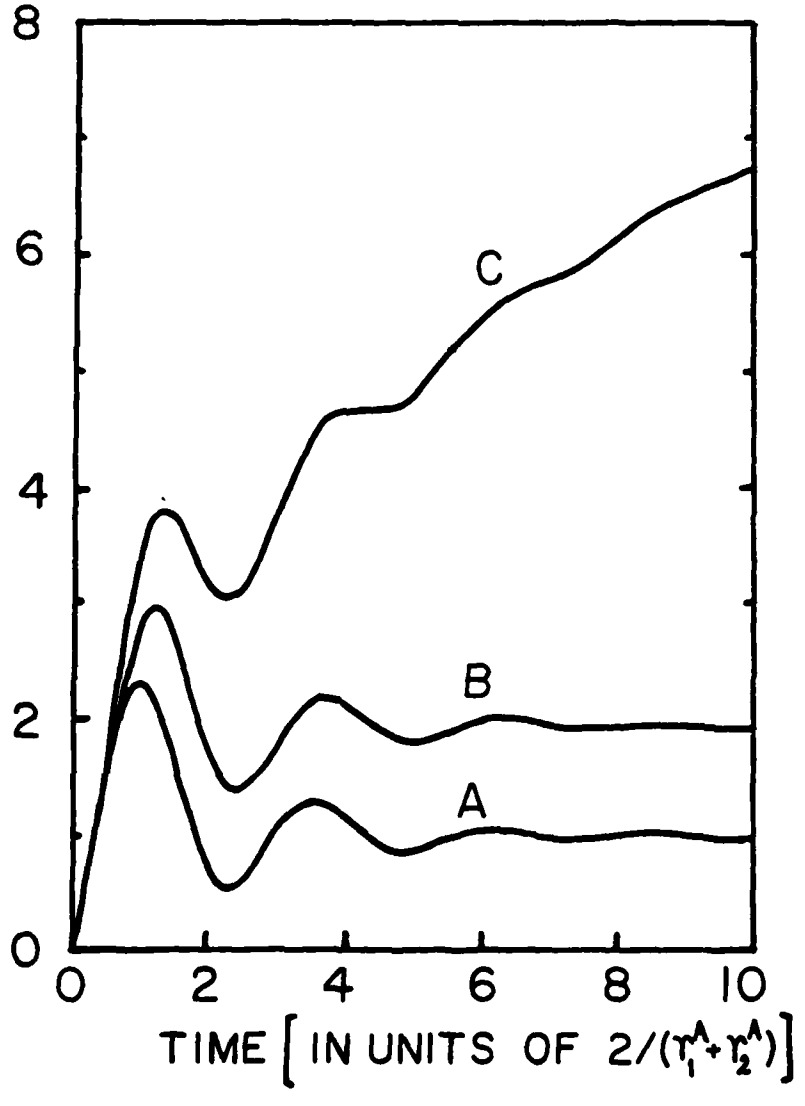

Fig.3

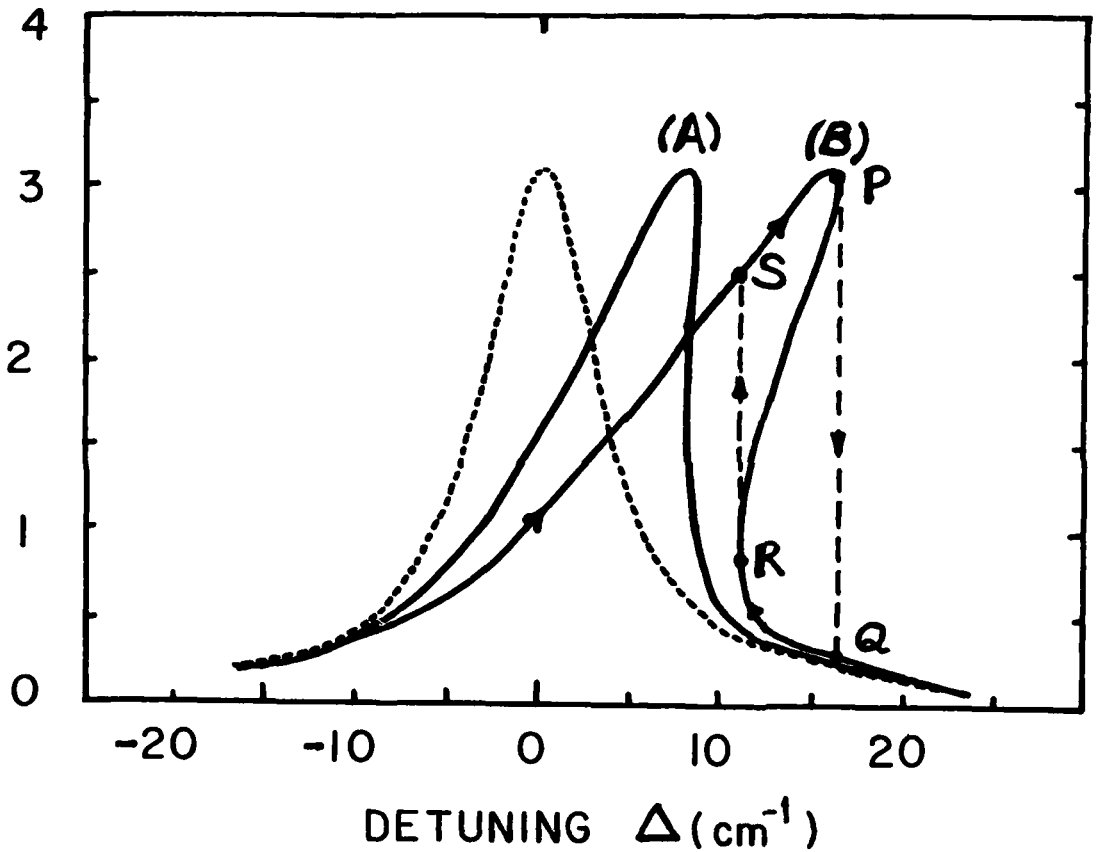

Fig. 4

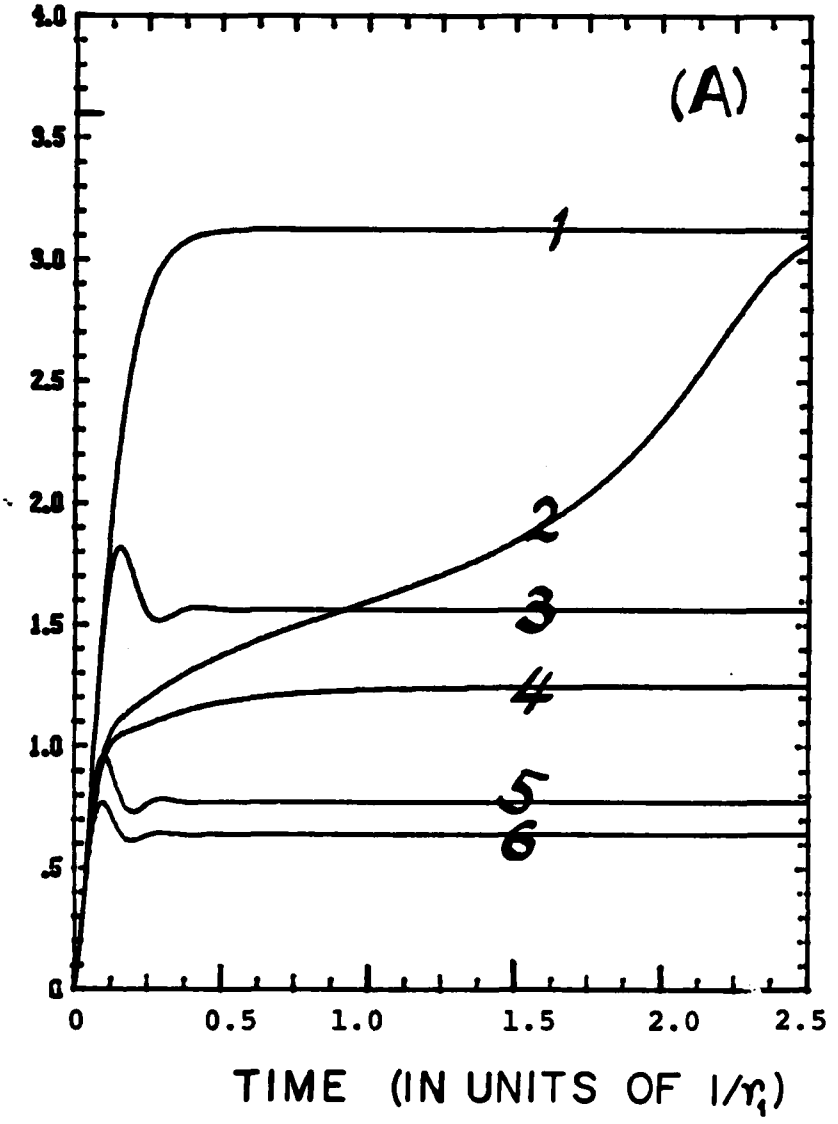
(A)
4.0
3.5
3.0
2.5
2.0
1.5
1.0
.5
0
0
0.5
1.0
1.5
2.0
2.5
1
2
3
4
5
6
TIME (IN UNITS OF $1/\gamma_1$)

Fig. 5(A)

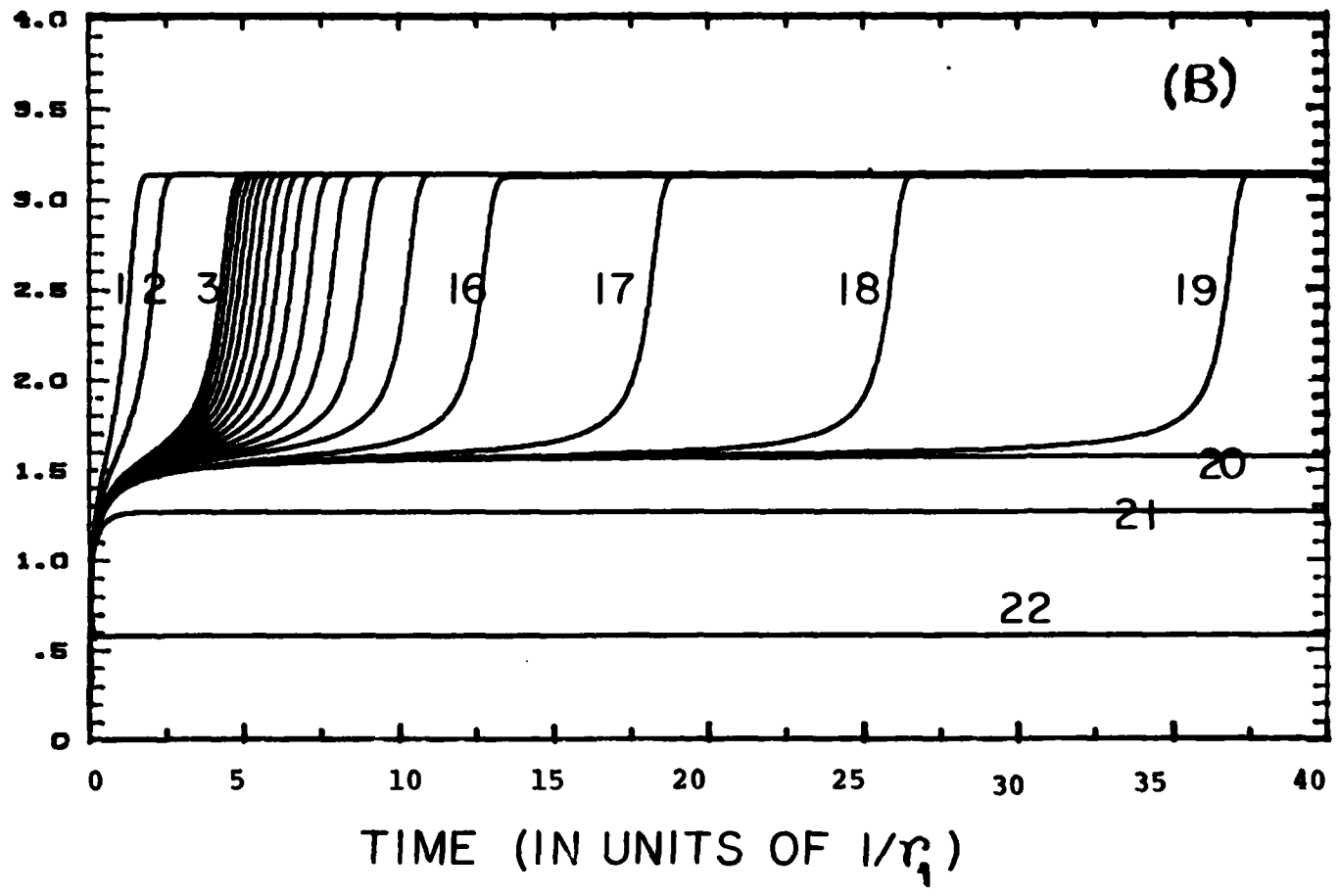
(B)
4.0
3.5
3.0
2.5
2.0
1.5
1.0
.5
0
1 2 3
16
17
18
19
20
21
22
0
5
10
15
20
25
30
35
40
TIME (IN UNITS OF 1/γ_1)

Fig. 5(B)

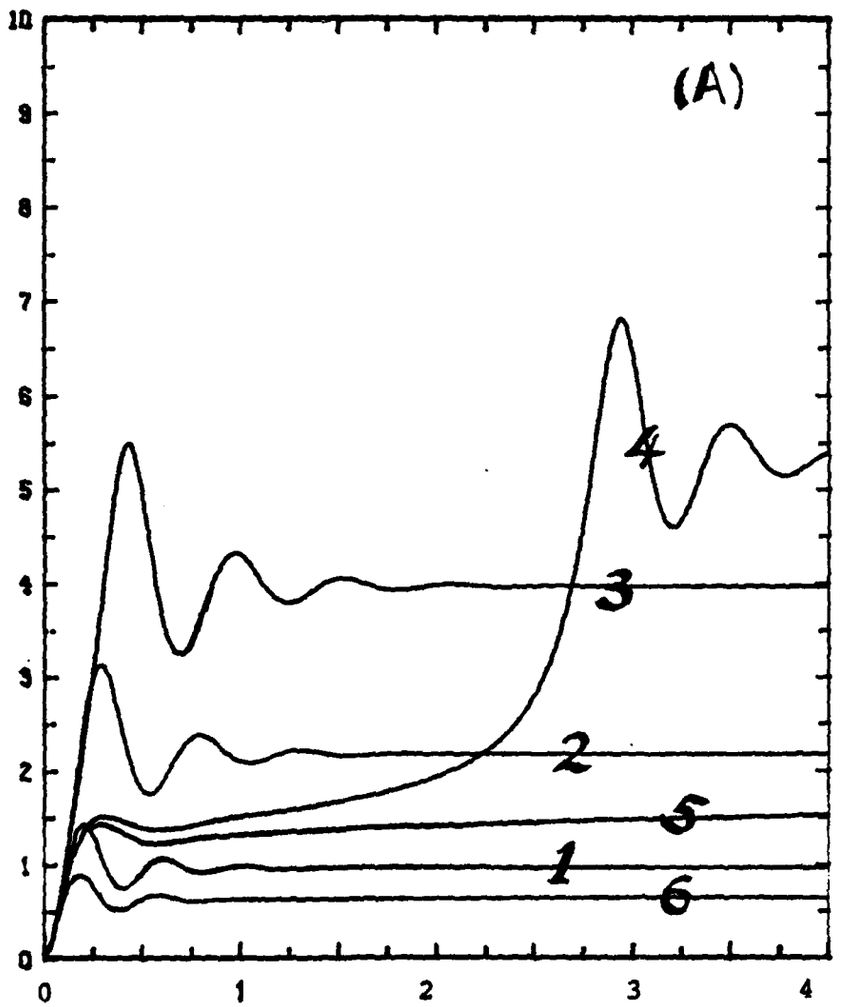

Fig. 6(A)

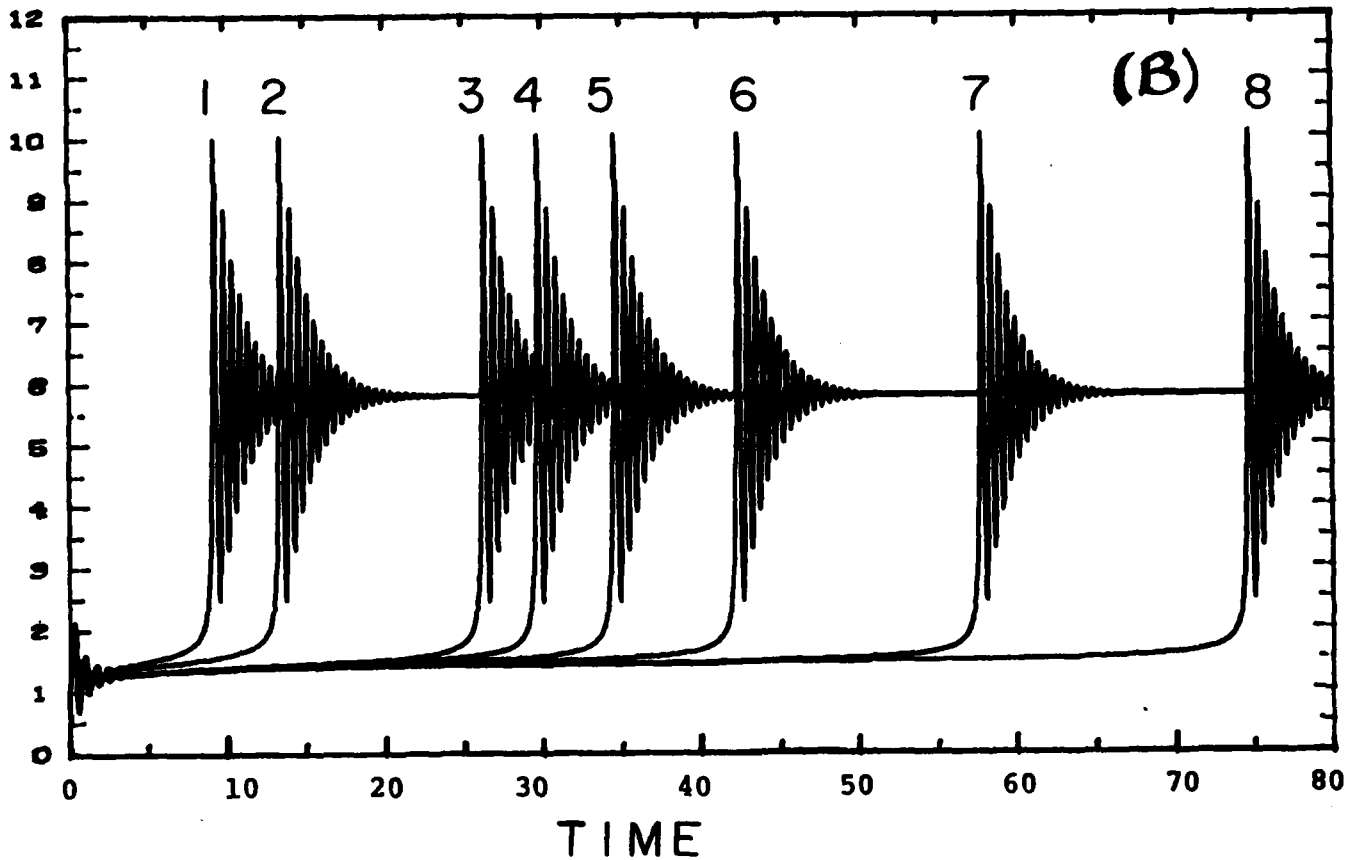

Fig. 6 (B)

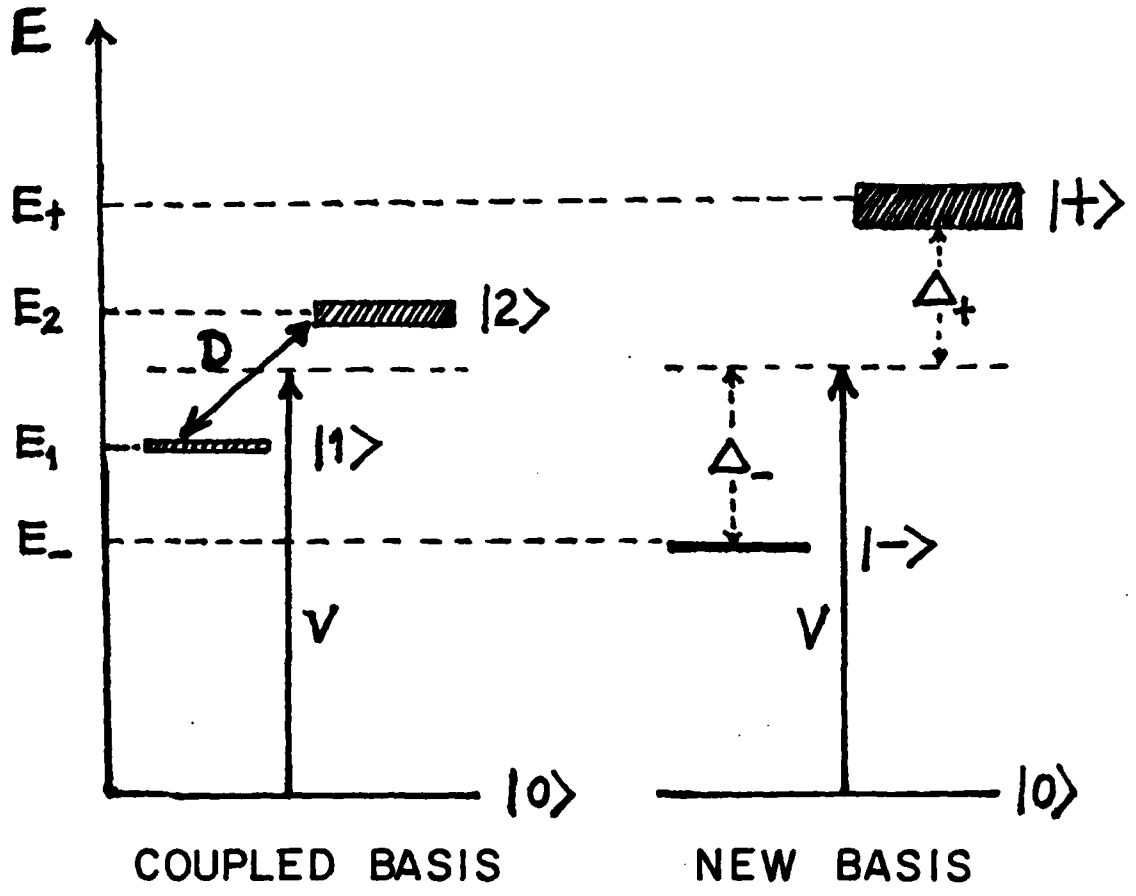

Fig. 7

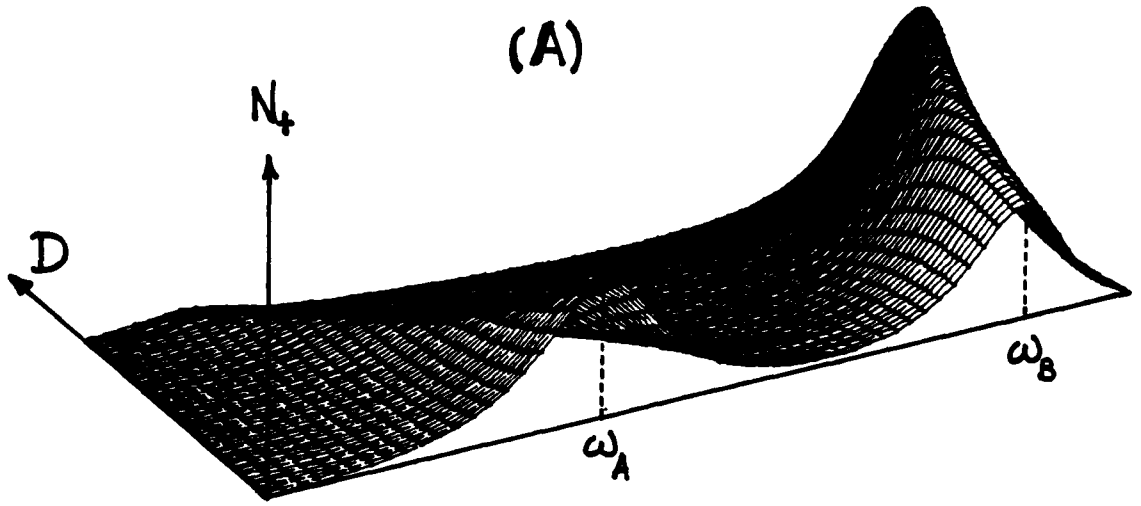

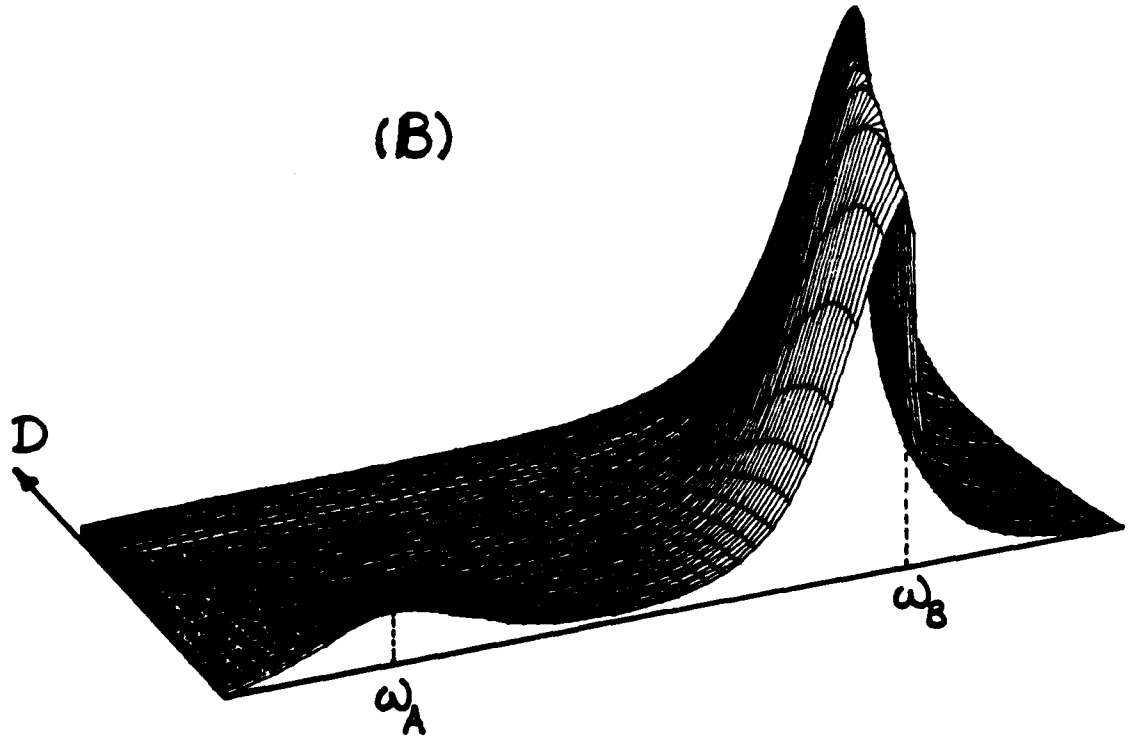

Fig 8. (A)&(B)

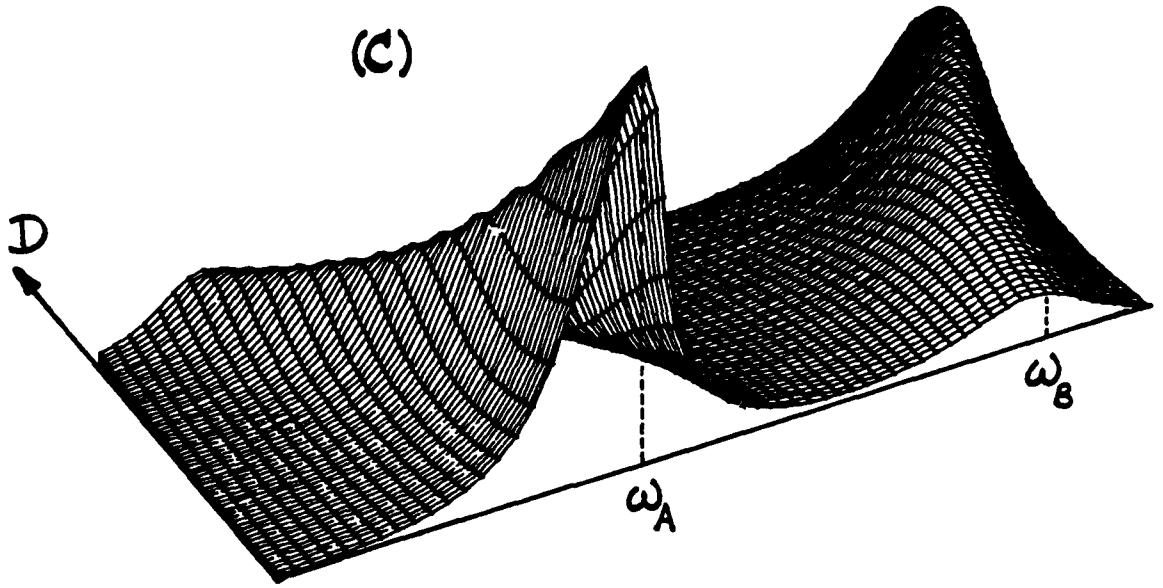

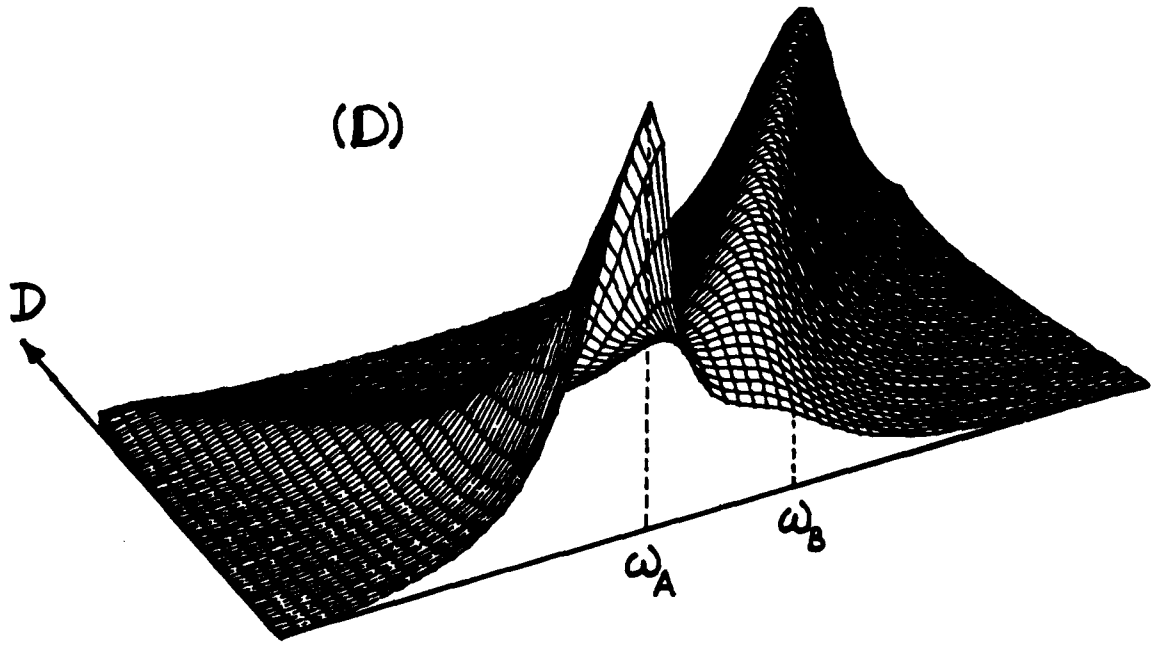

Fig. 8.(C)&(D)

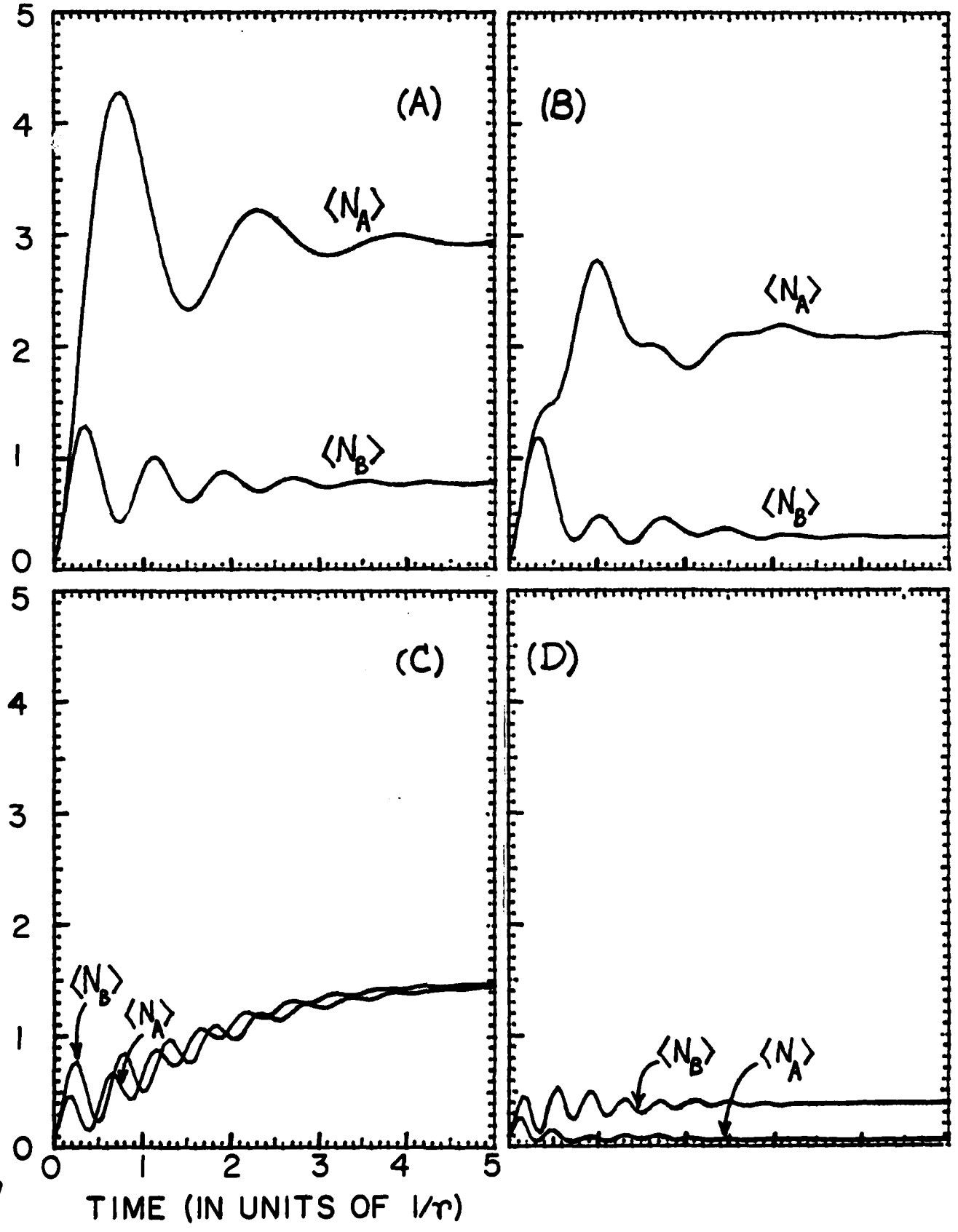

Fig. 9

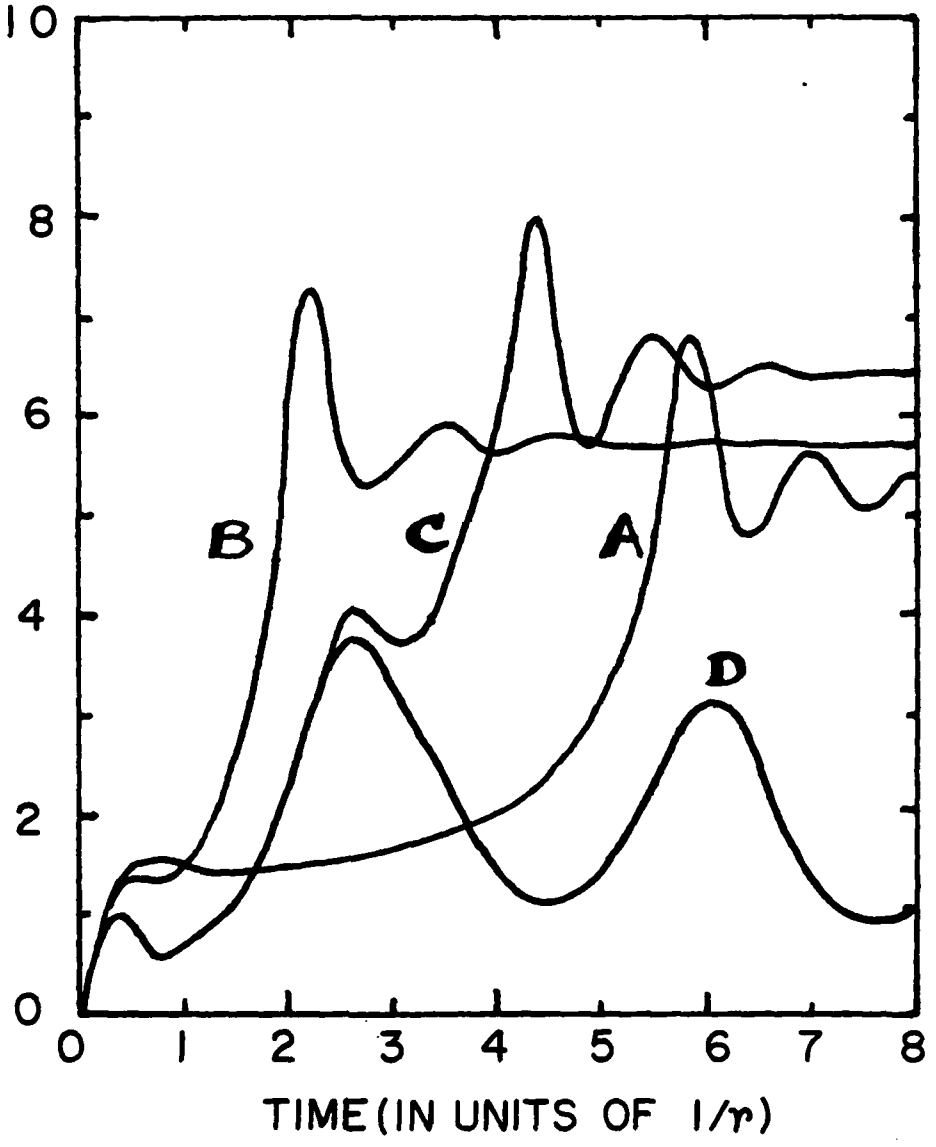

Fig. 10

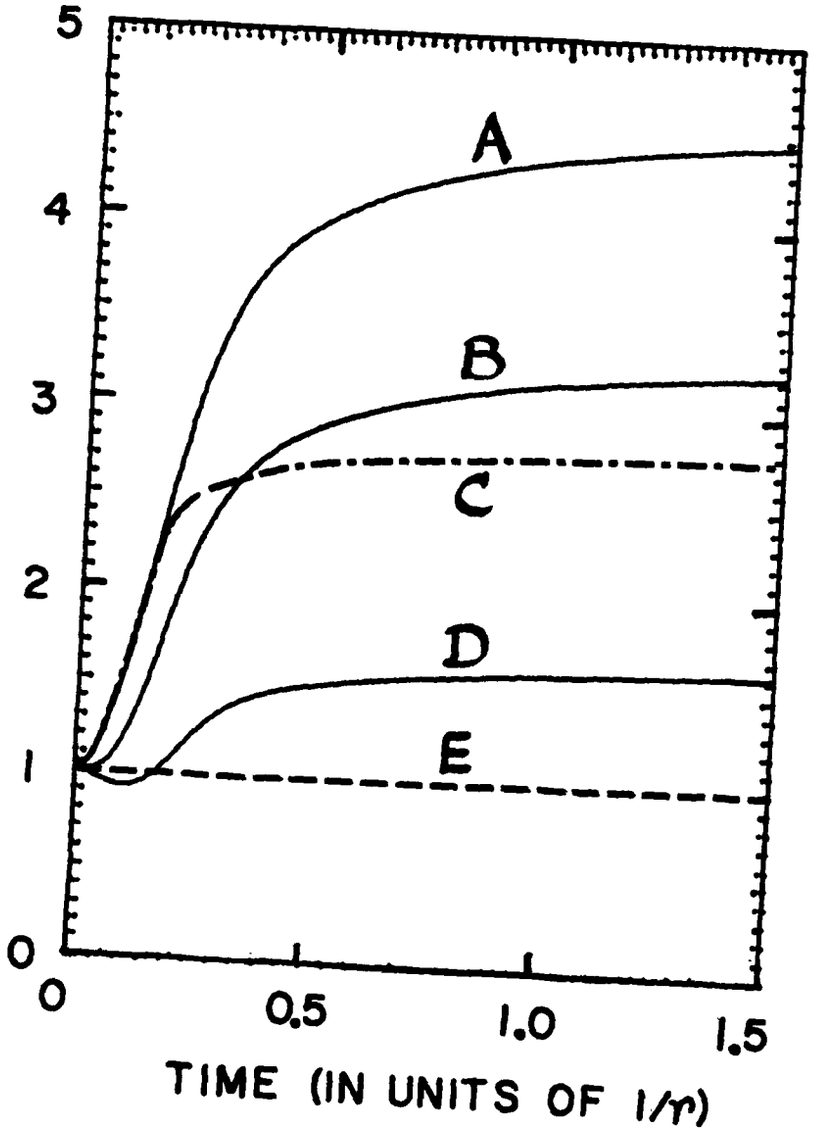

Fig. 11

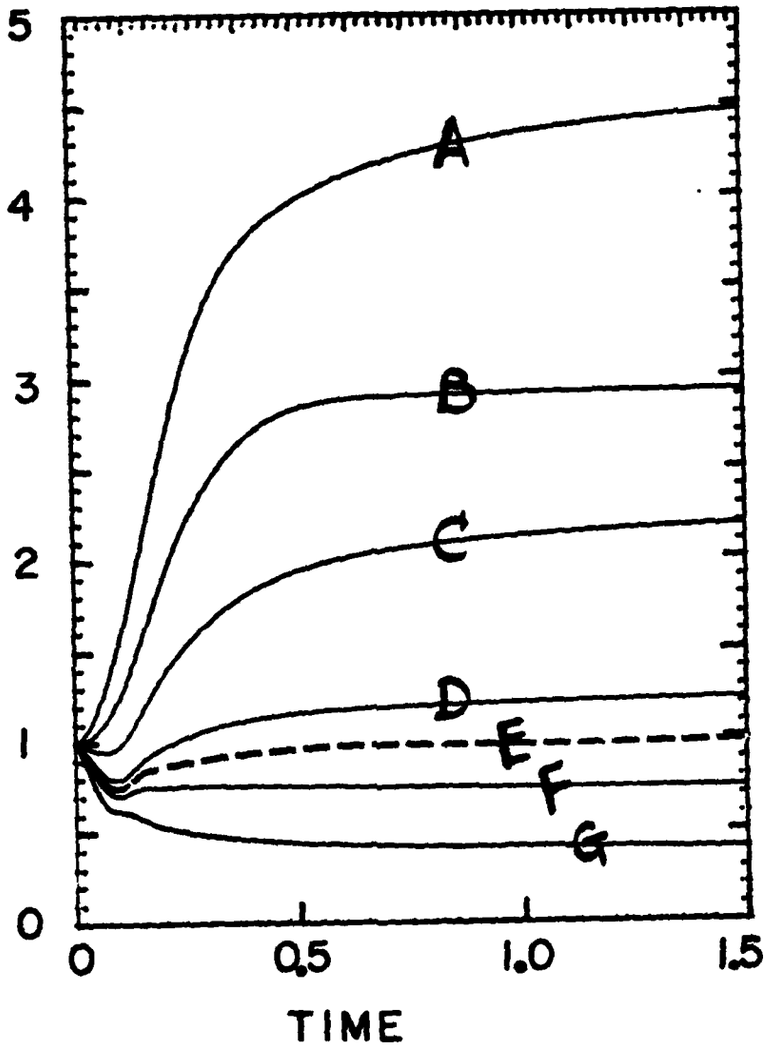

Fig. 12

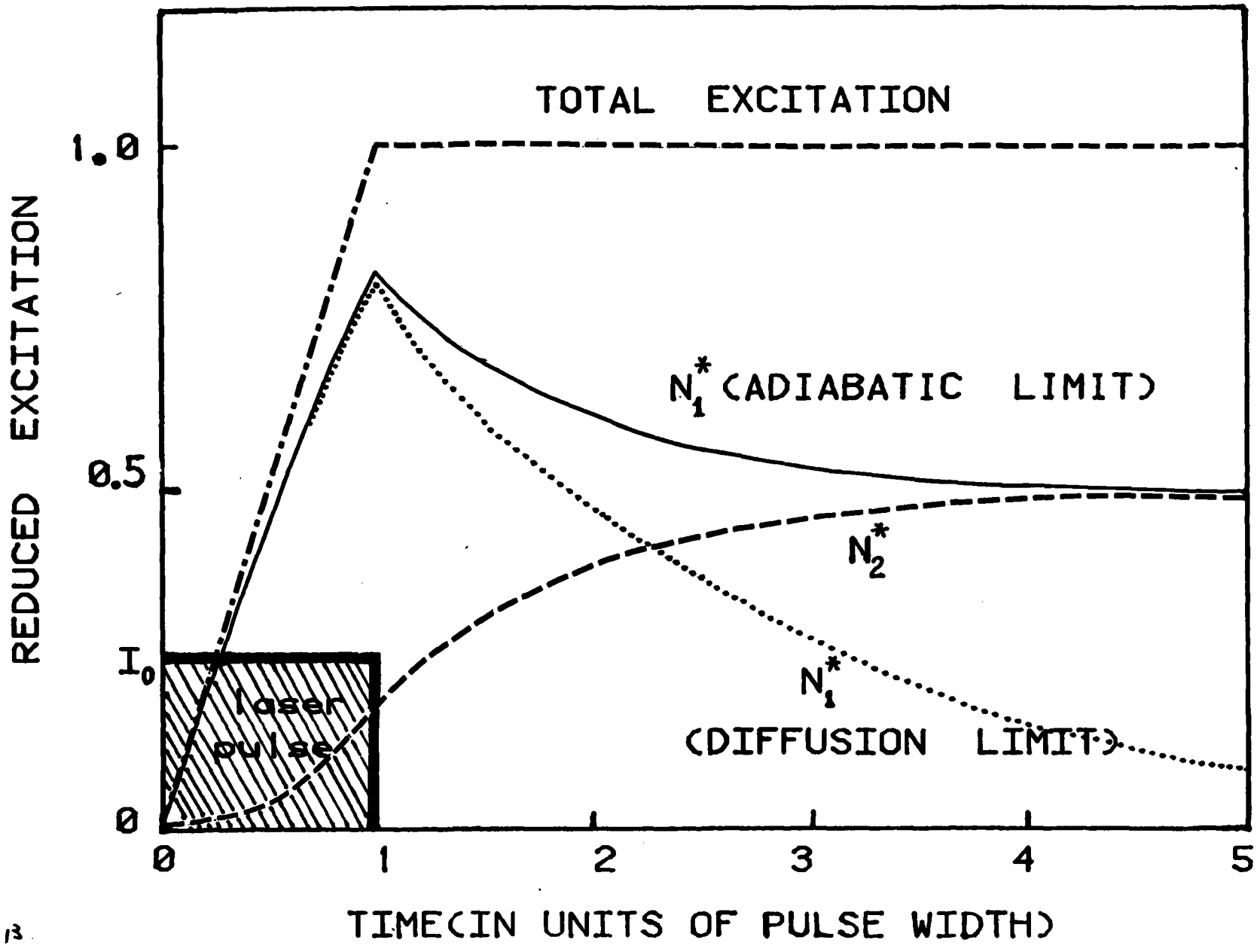
TOTAL EXCITATION
1.0
0.5
I_0
0
REDUCED EXCITATION
N_1^* (ADIABATIC LIMIT)
N_2^*
N_1^*
(DIFFUSION LIMIT)
laser pulse
0
1
2
3
4
5
TIME (IN UNITS OF PULSE WIDTH)

Fig. 13

SP472-3/A1

472:GAN:716:enj
78u472-608

TECHNICAL REPORT DISTRIBUTION LIST, GEN

	No. Copies
Office of Naval Research Attn: Code 472 800 North Quincy Street Arlington, Virginia 22217	2
ONR Western Regional Office Attn: Dr. R. J. Marcus 1030 East Green Street Pasadena, California 91106	1
ONR Eastern Regional Office Attn: Dr. L. H. Peebles Building 114, Section D 666 Summer Street Boston, Massachusetts 02210	1
Director, Naval Research Laboratory Attn: Code 6100 Washington, D.C. 20390	1
The Assistant Secretary of the Navy (RE&S) Department of the Navy Room 4E736, Pentagon Washington, D.C. 20350	1
Commander, Naval Air Systems Command Attn: Code 310C (H. Rosenwasser) Department of the Navy Washington, D.C. 20360	1
Defense Technical Information Center Building 5, Cameron Station Alexandria, Virginia 22314	12
Dr. Fred Saalfeld Chemistry Division, Code 6100 Naval Research Laboratory Washington, D.C. 20375	1
Dr. David L. Nelson Chemistry Program Office of Naval Research 800 North Quincy Street Arlington, Virginia 22217	1
U.S. Army Research Office Attn: CRD-AA-IP P.O. Box 12211 Research Triangle Park, N.C. 27709	1
Naval Ocean Systems Center Attn: Mr. Joe McCartney San Diego, California 92152	1
Naval Weapons Center Attn: Dr. A. B. Amster, Chemistry Division China Lake, California 93555	1
Naval Civil Engineering Laboratory Attn: Dr. R. W. Drisko Port Hueneme, California 93401	1
Department of Physics & Chemistry Naval Postgraduate School Monterey, California 93940	1
Scientific Advisor Commandant of the Marine Corps (Code RD-1) Washington, D.C. 20380	1
Naval Ship Research and Development Center Attn: Dr. G. Bosmajian, Applied Chemistry Division Annapolis, Maryland 21401	1
Naval Ocean Systems Center Attn: Dr. S. Yamamoto, Marine Sciences Division San Diego, California 91232	1
Mr. John Boyle Materials Branch Naval Ship Engineering Center Philadelphia, Pennsylvania 19112	1

SP472-3/A17

472:GAN:716:lab
78u472-608

TECHNICAL REPORT DISTRIBUTION LIST, 056

	No. Copies
Dr. G. A. Somorjai Department of Chemistry University of California Berkeley, California 94720	1
Dr. L. N. Jarvis Surface Chemistry Division 4555 Overlook Avenue, S.W. Washington, D.C. 20375	1
Dr. J. B. Hudson Materials Division Rensselaer Polytechnic Institute Troy, New York 12181	1
Dr. John T. Yates Department of Chemistry University of Pittsburgh Pittsburgh, Pennsylvania 15260	1
Dr. Theodore E. Madey Surface Chemistry Section Department of Commerce National Bureau of Standards Washington, D.C. 20234	1
Dr. J. M. White Department of Chemistry University of Texas Austin, Texas 78712	1
Dr. Keith H. Johnson Department of Metallurgy and Materials Science Massachusetts Institute of Technology Cambridge, Massachusetts 02139	1
Dr. J. E. Demuth IBM Corportion Thomas J. Watson Research Center P.O. Box 218 Yorktown Heights, New York 10598	1
Dr. C. P. Flynn Department of Physics University of Illinois Urbana, Illinois 61801	1
Dr. W. Kohn Department of Physics University of California (San Diego) LaJolla, California 92037	1
Dr. R. L. Park Director, Center of Materials Research University of Maryland College Park, Maryland 20742	1
Dr. W. T. Peria Electrical Engineering Department University of Minnesota Minneapolis, Minnesota 55455	1
Dr. Chia-wei Woo Department of Physics Northwestern University Evanston, Illinois 60201	1
Dr. D. C. Mattis Polytechnic Institute of New York 333 Jay Street Brooklyn, New York 11201	1
Dr. Robert M. Hexter Department of Chemistry University of Minnesota Minneapolis, Minnesota 55455	1
Dr. R. P. Van Duyne Chemistry Department Northwestern University Evanston, Illinois 60201	1

TECHNICAL REPORT DISTRIBUTION LIST, 056

	No. Copies
Dr. S. Sibener Department of Chemistry James Franck Institute 5640 Ellis Avenue Chicago, Illinois 60637	1
Dr. M. G. Lagally Department of Metallurgical and Mining Engineering University of Wisconsin Madison, Wisconsin 53706	1
Dr. Robert Gomer Department of Chemistry James Franck Institute 5640 Ellis Avenue Chicago, Illinois 60637	1
Dr. R. G. Wallis Department of Physics University of California, Irvine Irvine, California 92664	1
Dr. D. Ramaker Chemistry Department George Washington University Washington, D.C. 20052	1
Dr. P. Hansma Chemistry Department University of California, Santa Barbara Santa Barbara, California 93106	1
Dr. P. Hendra Chemistry Department Southampton University England SO9JNH	1
Professor P. Skell Chemistry Department Pennsylvania State University University Park, Pennsylvania 16802	1
Dr. J. C. Hemminger Chemistry Department University of California, Irvine Irvine, California 92717	1
Dr. Martin Fleischmann Department of Chemistry Southampton University Southampton SO9 5NH Hampshire, England	1
Dr. J. Osteryoung Chemistry Department State University of New York at Buffalo Buffalo, New York 14214	1
Dr. G. Rubloff I.B.M. Thomas J. Watson Research Center P. O. Box 218 Yorktown Heights, New York 10598	1
Dr. J. A. Gardner Department of Physics Oregon State University Corvallis, Oregon 97331	1
Dr. G. D. Stein Mechanical Engineering Department Northwestern University Evanston, Illinois 60201	1
Dr. K. G. Spears Chemistry Department Northwestern University Evanston, Illinois 60201	1
Dr. R. W. Plummer University of Pennsylvania Department of Physics Philadelphia, Pennsylvania 19104	1
Dr. E. Yeager Department of Chemistry Case Western Reserve University Cleveland, Ohio 41106	2
Professor D. Hercules University of Pittsburgh Chemistry Department Pittsburgh, Pennsylvania 15260	1

TECHNICAL REPORT DISTRIBUTION LIST, 056

	No. Copies
Professor N. Winograd The Pennsylvania State University Department of Chemistry University Park, Pennsylvania 16802	1
Professor F. George The University of Rochester Chemistry Department Rochester, New York 14627	1
Professor Dudley R. Herschbach Harvard College Office for Research Contracts 1350 Massachusetts Avenue Cambridge, Massachusetts 02138	1
Professor Horia Metiu University of California, Santa Barbara Chemistry Department Santa Barbara, California 93106	1
Professor A. Steckl Rensselaer Polytechnic Institute Department of Electrical and Systems Engineering Integrated Circuits Laboratories Troy, New York 12181	1
Professor R. D. Archer University of Massachusetts Chemistry Department Amherst, Massachusetts 01003	1
Dr. A. C. Pastor Hughes Research Laboratories 3011 Malibu Canyon Road Malibu, California 90265	1

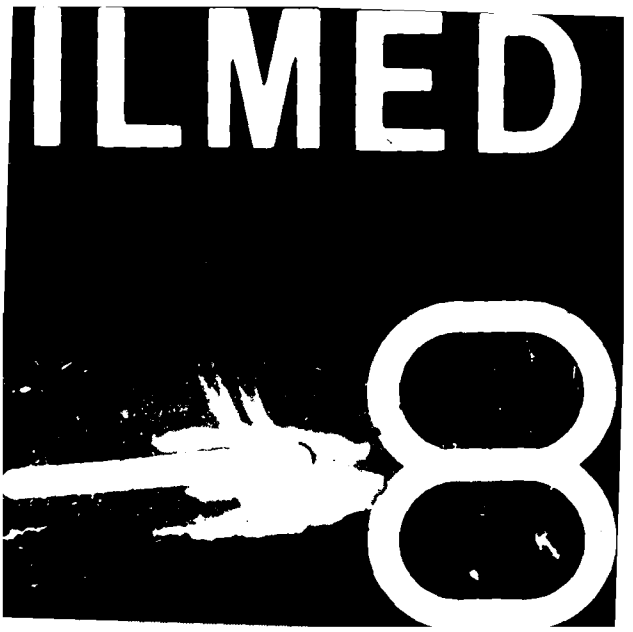
ILMED
8